Continental Shelf Research 262 (2023) 105028

Contents lists available at ScienceDirect

Continental Shelf Research

journal homepage: www.elsevier.com/locate/csr

26,000 years of environmental evolution of an incised valley in a rocky coast (La Janda wetland, SW Iberia).

Rosa Mediavilla [a], Juan I. Santisteban [b,*], Cristina Val-Peón [c], Luis Galán de Frutos [a], Margret Mathes-Schmidt [c], José A. López-Sáez [d], Francisco J. Gracia [e], Klaus Reicherter [c]

[a] C.N. Geological and Mining Institute of Spain, CSIC, C/Ríos Rosas, 23, 28003, Madrid, Spain
[b] Dept. Geodynamics, Stratigraphy and Paleontology, Complutense University of Madrid, C/José Antonio Novais, 12, 28040, Madrid, Spain
[c] Institute of Neotectonics and Natural Hazards, RWTH Aachen University, Lochnerstraße 4-20, 52060, Aachen, Germany
[d] Environmental Archaeology Research Group, Institute of History (CCHS), CSIC, Albasanz 26-28, 28307, Madrid, Spain
[e] Dept. of Earth Sciences, Faculty of Marine and Environmental Sciences, University of Cádiz, 11510, Puerto Real, Spain

ARTICLE INFO

Keywords:
MIS 1/3
Open and restricted estuaries
Gulf of Cádiz
Sea level
Tectonics
Stratigraphic architecture

ABSTRACT

The La Janda wetland record allows to expand the knowledge of the evolution of a restricted estuary since the Last Glacial Maximum. Multiproxy analysis of the sediments (facies, geochemistry, pollen, fossils) reveals that this system exhibits a classic incised valley sequence but differences with the adjacent estuaries can be established. The La Janda sedimentary infill can be split in four main sequences: (1) the Falling Stage Systems Tract (>20.6 ka BP) and (2) the Lowstand Systems Tract (16.7–20.6 ka BP) deposits record fluvial sedimentation in a narrow and incised valley, here seminally identified in the Gulf of Cádiz estuarine system; and (3) the Transgressive Systems Tract (7–16.7 ka BP), ending with the Holocene marine flooding surface at 7 ka BP, is composed of estuarine and marine basin deposits infilling a still steep and narrow topography coupled with the fast retreat of the river mouths. The (4) Highstand Systems Tract (0–7 ka BP) is composed of estuarine basin deposits with fluvial and tidal currents deposits in a wide a gentle sloped estuarine valley and it records the transformation of the basin into a terrestrial one. Comparison to other areas in the Gulf of Cádiz allows to correlate the different estuaries and to distinguish between open and restricted ones by the development of spit systems during the Highstand Systems Tract. But further work is needed to clarify the stratigraphy of the present eustatic cycle in the Gulf of Cádiz as the scarcity of data does not allow to determine the evolution of its estuaries during the last fall and rise of sea level. Such knowledge is crucial to disentangle the role of climate and tectonics in the future evolution of our coasts and design measures to adapt to sea level rise.

1. Introduction

Marine flooding of coastal areas due to increasing rate of sea level rise is one of the main risks linked to present climate change (Haasnoot et al., 2021; Nicholls et al., 2021; Strauss et al., 2021). This is one of the reasons why the analysis and comparison of recent examples of evolution of coasts is necessary. However, coastal systems are so complex and diverse that there is still a need to increase the knowledge on their dynamics and evolution.

Incised valleys and their sedimentary records are systems that supply valuable information about the environmental evolution of many coastal areas as a result of their main dependence on sea level changes (Zaitlin et al., 1994; Dalrymple et al., 1994; Allen and Posamentier, 1994) and, to a lesser extent, to direct climate change (Billeaud et al., 2009; Poirier et al., 2017) and recent human action (Cearreta et al., 2004, 2013; Evans, 2008). Beyond these allocyclic factors, autocyclic factors such as estuarine hydrodynamics (waves, tidal currents and fluvial supply), marine and terrestrial sediment availability and bed morphology (Chaumillon et al., 2008) play a fundamental role in their infill.

Of these autocyclic controls, hydrodynamics is the most influential and, consequently, wave or tide dominated estuaries are considered endmembers (Zaitlin et al., 1994; Boyd et al., 2006). However, there are many examples on which bed morphology play a key role on their hydrodynamics and sediment transport during the rise of sea level and their infill as the Bay of Biscay (Chaumillon et al., 2008; Allard et al.,

* Corresponding author.
E-mail address: j.i.santisteban@geo.ucm.es (J.I. Santisteban).

https://doi.org/10.1016/j.csr.2023.105028
Received 14 February 2023; Received in revised form 10 May 2023; Accepted 14 May 2023
Available online 16 May 2023

2010) and the Gulf of Cádiz (de Castro and Lobo, 2018). So, the infill of incised valleys in the same region or geological context, and under comparable sea level and climate conditions, can show a great variability (Menier et al., 2010).

The coastline of the SW Iberian Peninsula (between the Gibraltar Strait and Saint Vincent Cape) contains some well-studied records of incised valleys as the estuaries of the Guadalete (Dabrio et al., 2000; Lario et al., 2002), Tinto-Odiel (Borrego et al., 1999; Dabrio et al., 2000), Piedras (Borrego et al., 1993), Boca do Rio (Hindson et al., 1998), Quarteira (Schneider et al., 2010) and Guadiana (Morales, 1997; Lobo et al., 2003; Boski et al., 2008; Mendes et al., 2020) rivers. The common feature of these records is the prevalence of the hydrodynamics upon the bed morphology. However, La Janda lake is an incised valley resulting from the confluence of the Almodóvar and Barbate rivers in the Campo de Gibraltar region. This valley preserves the complete record of the complete last 26,000 years of an estuary controlled by the bed morphology, today transformed into a wide wetland area.

The aim of this paper is to describe and interpret the sedimentology and stratigraphy of the La Janda wetland using a sequential stratigraphy model (Catuneanu et al., 2011; Catuneanu, 2019) and the influence of the local and global factors in the sedimentation as well as the differences with the nearby coetaneous systems.

1.1. Geographic and geological setting

La Janda Basin (Hernández-Pacheco and Cabré, 1913) is located at the south of the Iberian Peninsula, near Vejer de la Frontera, 10 km away from the Atlantic coast (Gulf of Cádiz) and near 30 km from the Gibraltar Strait (Fig. 1a). It is a NW-SE fault-controlled depression (Goy et al., 1995; Zazo et al., 1999; Luque et al., 2001) almost 25 km in length and contains the wetlands and former lakes. Its lowest point is about 3 m a.s.l. (meters above sea level) while the highest surrounding areas are higher than 400 m a.s.l. Present-day basin is crossed and drained by the Barbate River along the western limits of the lake basin, and also by other tributaries, Almodóvar and Celemín rivers, being heavily disturbed by farming activities. After crossing the basin, the Barbate River flows to the west and then dramatically changes its trace to the SE (Fig. 1b), running to the sea through a narrow gorge and flowing into a marsh complex with a tidal range of c. 2 m (Instituto Hidrográfico de la Marina, 2019). The Mediterranean-Atlantic climate of the region is characterized by an annual average rainfall of c. 850 mm, mostly during winter months, and mean annual temperatures from 16 °C to 19 °C and a thermal range between 10 and 16 °C. Easterly prevailing winds are frequently followed by W and SW winds (Dueñas López and Recio Espejo, 2000).

La Janda is placed in the convergence area of the Eurasian-African plates, at the westernmost sector of the Betic Cordilleras and in the Gibraltar Arc structure, being subjected to an intense tectonic activity during Cenozoic times (Benkhelil, 1976; Sanz de Galdeano, 1990; Azañón et al., 2002).

From Burdigalian until Tortonian, the Gibraltar Arc uplifted under a WNW-ESE compressive stress field (Balnayá and García Dueñas, 1988; Leblanc, 1990; Sanz de Galdeano, 1990; Vergés and Fernández, 2012; González-Castillo et al., 2015). Since then, and until recent times, the stress field has rotated to NW-SE to NNW-SSE direction (Benkhelil, 1976; Sanz de Galdeano, 1990; Goy et al., 1995; Zazo et al., 1999; Gracia et al., 1999; Reicherter and Peters, 2005).

The geology of the Gibraltar Arc in the studied area is composed by siliciclastic and carbonated pre- and synorogenic turbiditic deposits (Almarchal, Algeciras and Aljibe Series of the Gibraltar Flysch), spanning from Late Cretaceous to Middle Miocene times, affected by thrusts, backthrusts and dextral strike-slip faults (Hernaiz Huerta et al., 1991). Upper Miocene-Pliocene postorogenic sediments consist of breccias, calcarenites and siliciclastic marine deposits filling subsiding troughs affected by Plio-Pleistocene compressive tectonics (García de Domingo et al., 1991; Goy et al., 1995). The distribution of Quaternary deposits is controlled by neotectonics, being preferential along the present coastline of the Gibraltar Strait (Rodríguez Vidal et al., 2004), fluvial valleys

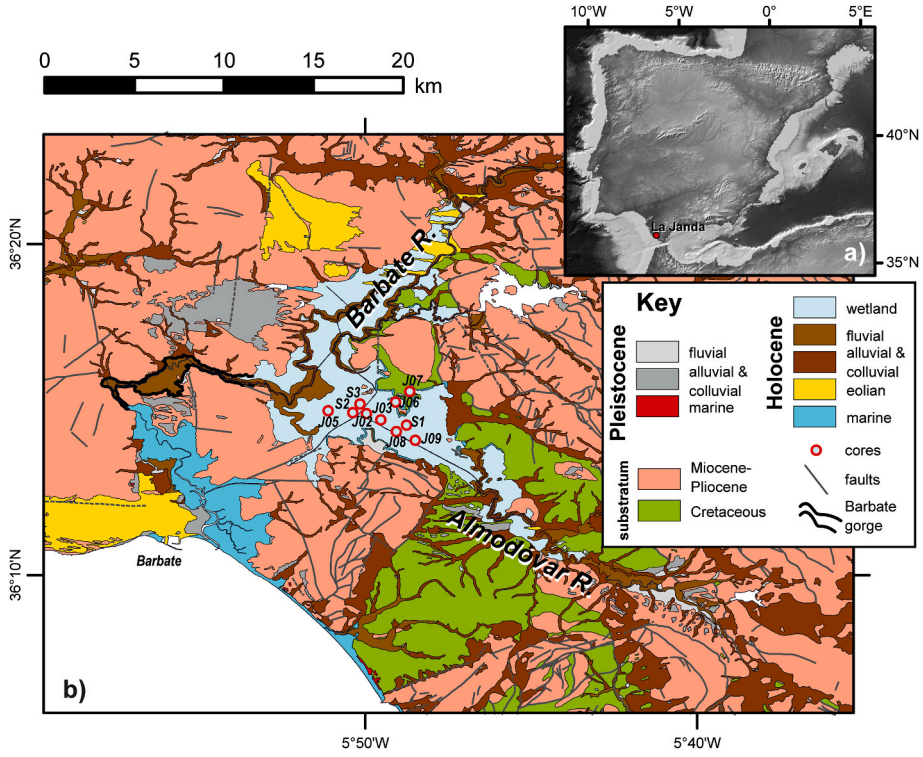

Fig. 1. (a) Location of the studied area. (b): Geological map of La Janda basin and borders, simplified from the Continuous Geological Map of Spain 1:50.000 (GEODE). Geographical data provided by the Spanish Geographical Institute (IGN) and the geological map by the Instituto Geológico y Minero de España, CSIC (Roldán et al., 2021).

and the La Janda basin (Fig. 1b).

Luque et al. (1999) found estuarine siliciclastic deposits, dated as 3810 cal. BP, at −5 m a.s.l. revealing that the basin was below sea level. Later basin infill led to the isolation from the sea and the beginning of alluvial and, afterwards, lacustrine sedimentation (Luque et al., 1999, 2001; Dueñas López and Recio Espejo, 2000).

2. Methods

In 2016 and 2017 twelve cores were recovered in two coring campaigns by triple barrel system (cores S1, S2 and S3) and a portable Ejkelkamp and Atlas Copco vibracoring systems (cores named JAN), all of them encased in PVC or methacrylate pipes (Table 1). The cores were split in two in the laboratories of the Spanish Geological Survey (IGME, CSIC), and one half was stored as an archive, whilst the other half was used for description, analyses and sampling. All of them were photographed, their sedimentary features were described and stratigraphic logs (scale 1:20) were elaborated correcting the depths to remove the effect of compaction due to drilling.

2.1. Physical properties and mineralogical and geochemical composition of the sediments

Non-destructive analyses were run on the cores, at the laboratories of the Spanish Geological Survey (IGME, CSIC), including.

- Core colour scan (high resolution images with a down core resolution of 50 μm) with a Geoscan IV coupled to the MSCL GEOTEK.
- Colour (RGB) analyses were performed with 1 mm down core resolution using a Konica Minolta 700-d spectrophotometer integrated in the GEOTEK XRF core scanner. Each channel had values ranging from 0 up to 255 and a R/(G + B) colour index was used to represent the dominant tones (red/brownish against green/greyish) and a (R + G + B)/3 index represents the grey scale range.
- Geophysical properties (P-wave velocity, gamma density, non-contact resistivity and magnetic susceptibility) were analysed with 1 cm down core resolution with a GEOTEK Multi-Sensor Core Logger (MSCL-GEOTEK).
- XRF scanning with a GEOTEK XRF core scanner in a He purged atmosphere with an illumination window of 15 mm (cross-core slit width) x 10 mm (down-core resolution). Two runs, with 30 s count time exposure, were performed for 10 kV and 40 kV (detecting from Mg to U). XRF spectra were processed with bAxil. Element intensities are represented in counts per second (cps).

Sampling was carried out in cores S2 and S3 to characterize the sedimentary facies at the IGME laboratories.

- Mineralogical analysis by X-ray diffractometry (PTE-RX-04) for bulk sample and <2 μm fraction. These analyses were used to check the sources of the chemical elements obtained from geochemical analyses.

Table 1
Location of cores. Bold: cores presented in this paper (see location in Fig. 1b).

Core	Latitude	Longitude	Height (m a.s.l.)	Length (m)
S1	36°14′29.62″ N	5°48′44.33″ W	4.11	10.00
S2	36°14′53.88″ N	5°50′21.45″ W	4.88	27.50
S3	36°15′09.68″ N	5°50′08.52″ W	5.50	26.78
JAN-02	36°14′53.63″ N	5°49′57.24″ W	4.81	3.00
JAN-03	36°14′40.76″ N	5°49′31.26″ W	3.65	13.50
JAN-05	36°14′57.61″ N	5°51′06.16″ W	4.80	13.00
JAN-06	36°15′13.62″ N	5°49′04.22″ W	5.28	2.00
JAN-07	36°15′31.68″ N	5°48′38.85″ W	8.23	3.00
JAN-08	36°14′19.82″ N	5°49′03.65″ W	3.67	3.00
JAN-09	36°14′03.80″ N	5°48′28.39″ W	4.28	13.00

- Geochemical analysis of major oxides and trace elements by X-ray fluorescence and atomic absorption spectroscopy (XRF and AAS). The results were used to check the validity of the non-destructive high-resolution XRF scanning.
- Carbon (C) (organic, inorganic and total) and sulphur by elemental analyser (ELTRA). S data was used to check the results of XRF core scanning. Carbon values gave an estimate of organic matter and carbonate content, and they can be compared to other results from non-destructive techniques (XRF core scanning and colour).

2.2. Dating and age-depth model

A total of 25 samples (cores JAN05A, S2, S3, JAN09A) were ^{14}C-dated (Beta Analytic Inc., USA and Keck Carbon Cycle AMS Facility at UC Irvine, USA). Calibration was performed with CALIB 8.2 (Stuiver et al., 2021) using the IntCal20 and Marine20 calibration datasets (Reimer et al., 2020; Heaton et al., 2020) and different reservoir effect values (Table 1). These reservoir effects/values have been recalculated based on the literature (Soares and Dias, 2006; Soares and Martins, 2010; Martins and Soares, 2013) and using the web application of Reimer and Reimer (2017) following the methodology of Soulet (2015).

Due to the peculiar setting of the sediments (in a restricted and shallow environment) several calibration sets were developed to check which calibration curve and reservoir effect values (if applied) were the best. Bchron (Haslett and Parnell, 2008), clam (Blaauw, 2022), rbacon (Blaauw and Christen, 2011), rcarbon (Crema and Bevan, 2021) and a simple lineal interpolation were used to build a reliable age-model.

2.3. Pollen analysis

Sampling for palynological analyses was undertaken as follows: 52 test-samples were collected from core S2 at different intervals and 160 samples were collected from core S3 maintaining a regular interval of 10 cm. All samples were chemically treated with HCl (10%) to remove carbonates, KOH (10%) to remove humic acids, and Sodium Polytungstate (SPT: 3Na2WO4·9WO3·H2O) at 2.0–2.1 gr/cm^3 for densimetric separation. The final residue was mounted on slides with the use of glycerol. Pollen concentrations (grains/gr of dry sediment) were estimated by adding two *Lycopodium clavatum* tablets to each sample (Stockmarr, 1971). Palynomorphs were counted using an optical microscope at 400x and 1000x up to a minimum pollen sum of 300 terrestrial pollen grains. Palynomorphs were identified using published keys (Moore et al., 1991; Reille, 1992, 1995; Van Geel, 1978, 2001; Van Geel et al., 1980, 1986, 1989, 2003).

For the purpose of this paper, three well-represented palynomorphs were selected as good ecological indicators of specific environments related to the study area (Fig. 2a, 3a and 3b). Species from the Chenopodiaceae family grow in temporary pools of brackish or saline water, the edges of lagoons, the open spaces of coastal marshes, and areas affected by tides (Domínguez et al., 1993; Galán de Mera et al., 1997; Latorre et al., 1996; Rivas-Martínez et al., 1997); hence, it is used here as a good marker of marine influence. *Isoetes* typically grows in shallow waterlogged environments associated to fresh water marsh communities, usually with oligotrophic waters (Cirujano et al., 2014); thus, it is used as an indicator of environments with a progressive loss of marine influence. *Glomus* (HdV-207) is associated to processes related to the development of new soils, soil erosion from watersheds, dry or desiccated areas, and farming activities (Anderson et al., 1984, 2011; López-Sáez et al., 2000; van Geel et al., 1989); therefore, it is considered a marker of erosive processes of different nature.

Concentrations and percentages were calculated using TiliaIT software (version 2.1.1, Illinois State Museum, Research and Collection Center, Springfield USA). Percentages were calculated considering a terrestrial pollen sum (TPS) that excluded aquatic pollen types, which were included in the total sum (TS) together with Non-Pollen Palynomorphs.

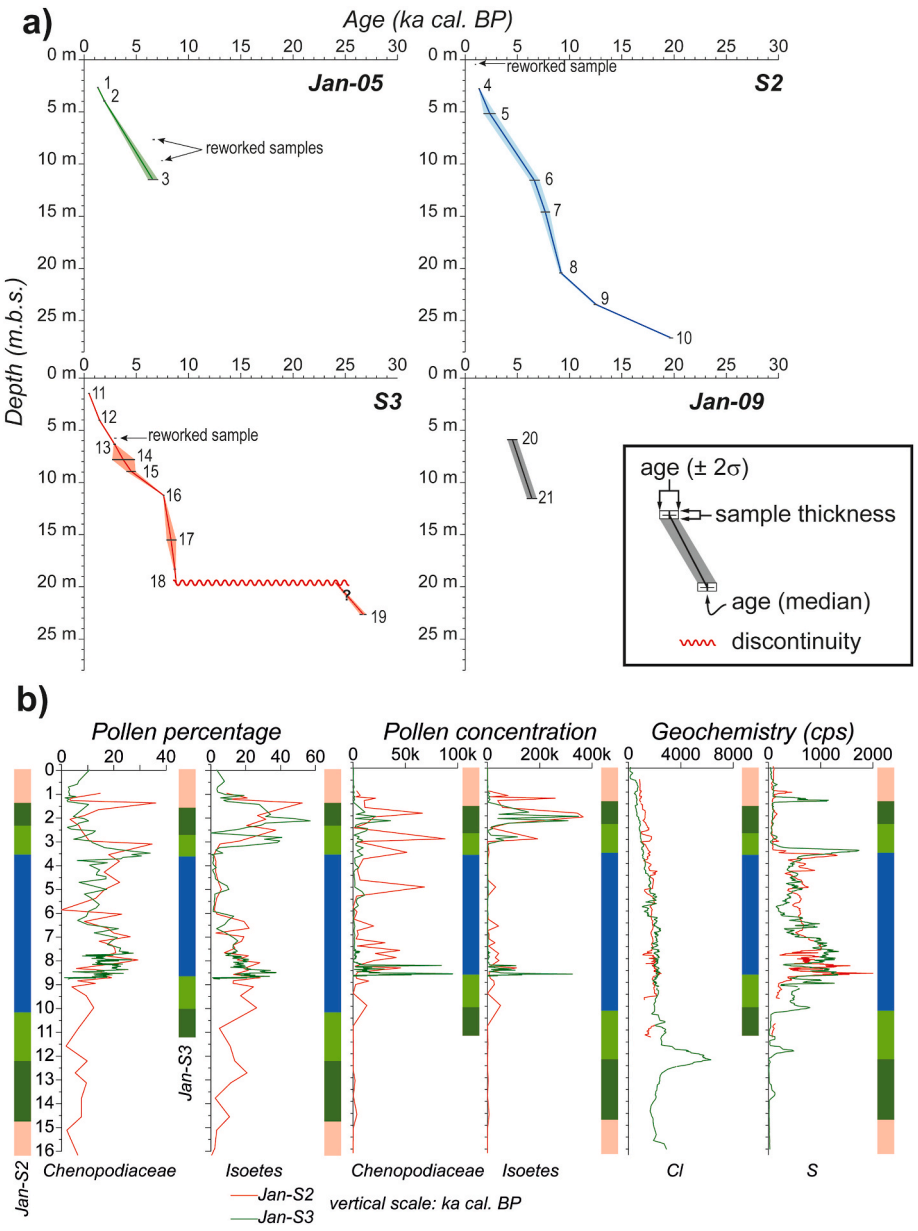

Fig. 2. Age models for (a) cores S2, S3, JAN-05A and JAN-09A. The numbers for reference are those of Table 2. (b) Comparison of age-depth models for cores S2 and S3 based on pollen and geochemistry. Vertical colour bars: see Fig. 3 key.

3. La Janda record

3.1. Age-depth model

Before applying the different age models to the dated samples, four samples were rejected as, presumably, they contain reworked carbon (Table 2).

Several age-depth models were discarded based on inconsistencies (age reversals, unreasonable sedimentation rates, etc.) and, for the remaining ones, the simplest one, a simple lineal model (Fig. 2a), was applied to the cores for further checking by comparison of different proxies among cores (Fig. 2b).

Despite their similarity, age-depth models for the different cores cannot be combined in a single one as differences in sedimentation rates caused artifacts that result in unrealistic correlations.

Cores S2 and S3 show the longest records, ca. 20 ka BP for core S2 and ca. 27 ka BP for core S3. They begin with low sedimentation rates during the late Pleistocene. For core S3 this is interrupted by a discontinuity while core S2 record is continuous and it shows a gradual increase in sedimentation rate at the end of the Pleistocene.

The Holocene record starts with high sedimentation rates for cores S2 and S3 until ca. 7 ka BP, when the sedimentation rate for all cores, except JAN-09, decreases. The greater rates for core JAN-09 can be due to its proximity to a river mouth, which increased the supply of sediment at this location.

Despite the noticeable decrease in sedimentation rate for the last 7 ka, in comparison to the 7 to 9 ka BP period, it is worth to notice that sedimentation rates increased slowly until present.

3.2. Facies analysis

Facies have been characterized by visual inspection as well as by their geophysical properties, geochemical and mineralogical composition. Such parameters show both gradual and abrupt changes and, therefore, we describe the logs and then the Facies Groups (which are composed of different facies but grouped in a larger set). These groups

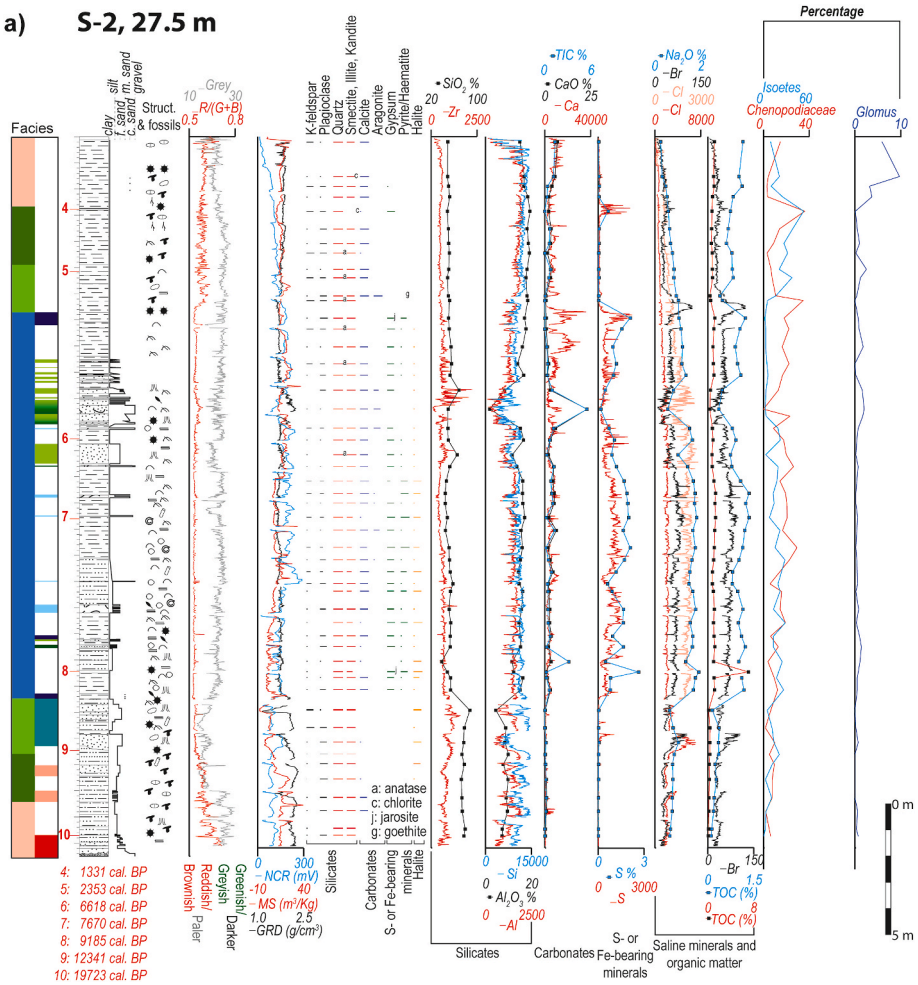

Fig. 3. Sections for cores (a) S2 and (b) S3 showing selected parameters: facies and subfacies, dated samples (numbers from Table 2), lithology, grain size, structures and fossil content, colour and geophysical logs (resistivity, magnetic susceptibility [MS], gamma ray density [GRD], non-contact resistivity [NCR]), mineralogy [relative abundance: width of the bars, thickness of the sample: height of the bars], selected oxides and inorganic (TIC) and organic (TOC) carbon (in percentage) and geochemical XRF scan (in counts per second) and selected pollen and non-palynomorph taxa as percentages and concentrations. (c) Sedimentary model and identified subfacies. m: mud, s: sand, p: pebble, g: granule, c: cobble, sd: shell debris, sh: shells, ch: charcoal, sl: shell in living position.

are the basis for the environmental interpretation.

3.2.1. Geophysical logs

Due to the homogeneity of the sediments, the more distinctive logs are those of colour that can be linked to their oxidation or reduction degree and composition.

The lowermost materials show higher values of the R/(G + B) and Grey indexes, indicative of warm pale tones. Similar R/(G + B) values can be observed at the top of the sections, but, in this case, the Grey index points to darker tones. Between these levels, the R/(G + B) and Grey indexes fall except for some intercalations that show paler tones, and sometimes more ochre, coincidental with coarser siliciclastic levels.

The colour of the sediments is indicative of their oxidation level (Lyle, 1983; Nagao and Nakashima, 1992). Thus, brown and ochre colours are indicative of oxidizing conditions typical of emerged setting. The appearance of green to grey colours implies reductive processes by consumption of the bottom oxygen (submerged conditions) while the mixture of colours (mottling) indicate alternating conditions.

The remaining parameters (gamma ray density, magnetic susceptibility and resistivity) are dependent on the mineralogical composition and grain size of the sediment. Due to the dominance of clay minerals, the profiles are very homogeneous and they only show changes where coarser grain siliciclastic or mixed siliciclastic-bioclastic levels appear. In such cases, the three parameters increase their values for siliciclastic coarser grain size levels but not for bioclastic levels.

The geophysical proxies are indicative of the grain size and composition of the sediments and, thus, they provide information about the energy of the environment. In this case, the general sedimentation is fine grained, pointing to a sedimentation from suspension, with some coarse-grained deposits, more energetic, intercalated among them. The composition of these more energetic levels can be siliciclastic, bioclastic and mixed, indicating a mixture of provenances that are exogenous (siliciclastics) and autochthonous (bioclastic). Such episodes can be then linked to external inputs to the basin (from rivers) and the reworking of the bottom of the basin by waves or currents.

3.2.2. Geochemistry and mineralogy

The studied sediments are composed by siliciclastics (mostly mud with some levels of sands and gravels) with contributions of carbonates (nodules and shells, sparse or in levels) and disseminated organic matter, gypsum, pyrite and halite (Fig. 3). Thus, the geochemical composition of these materials is controlled by this mineralogical composition. Some elements are shared between minerals, but major components represent most of the content of the main ions. As an example, Calcium (Ca, CaO) can be present in carbonates, gypsum and some silicates. However, the good correlation with total inorganic Carbon (TIC)

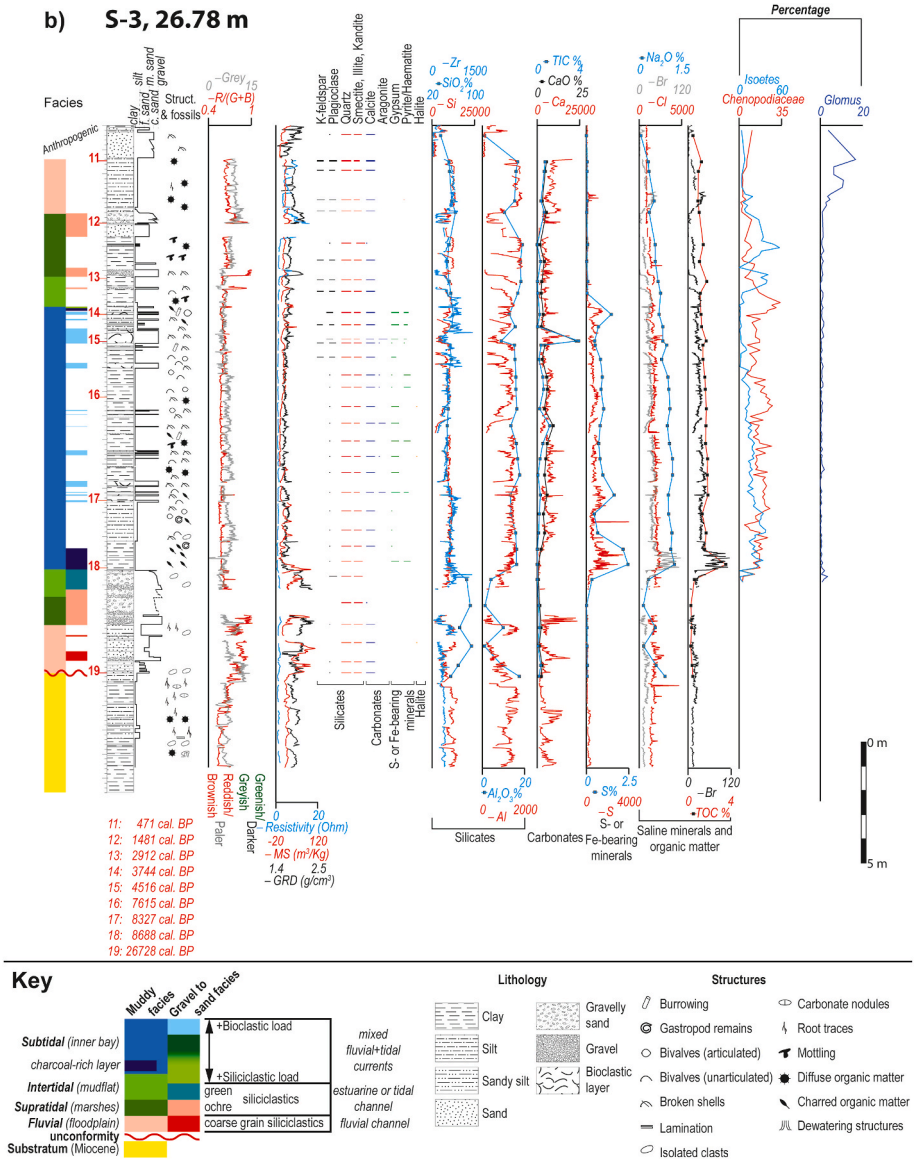

Fig. 3. (*continued*).

indicates that most of it is linked to the carbonates. However, Sulphur (S) is mainly linked to the presence of gypsum and/or pyrite, pointing to the minor contribution of these minerals to the bulk composition of the sediments.

Another question is the difference in techniques. As pointed by several authors, the XRF scanning is usually applied on wet sediments and the water content can affect the results, which can be different to those obtained by classical "destructive" techniques in which the sample is grounded, desiccated and homogenized (Tjallingii et al., 2007; Dunlea et al., 2020). For this reason, in addition to the XRF scanning a selection of samples from cores S2 and S3 (the longest ones) were analysed by ICP spectrometry and AAS.

The results of these mineralogical and geochemical analyses are shown in Fig. 3 (a, b) and reveal the good agreement among the mineralogical, "classical" geochemical analysis and XRF scanning.

Sometimes, the facies show clear changes in the composition, but also there are gradual changes.

The siliciclastic components (exogenous component) are best described by the content in silicon (Si), aluminum (Al), zirconium (Zr) and titanium (Ti). Si is shared by all of them, but it increases with the amount of quartz, as well as Zr, being noticeable at coarser levels. Al is shared by clay minerals and feldspars, but being the latter less present, its content can be ascribed to the clay content. Thus, volume changes of these elements reflect changes in the ratio exogenous/endogenous minerals and in grain size (energy). The composition in the cores is very homogeneous except where gravel and sandy layers appear and the relative Al content decreases. Due to the highest intensity of Al peaks, the sandy levels rich in matrix are masked.

The endogenous components are carbonates, gypsum, halite and pyrite/haematite. These are of terrestrial or marine origin.

The carbonates are recorded by TIC, which correlates to Ca and CaO. They are present in two components: nodules and forming part of the matrix (edaphic) and shells (entire or broken, marine and transition). The edaphic carbonate is recorded by a background Ca content without noticeable peaks. The marine carbonate content is larger on the average and conspicuous peaks corresponding to shells (isolated or in levels) are observed.

The content in sulphur (S) varies with gypsum and pyrite content, but also with total organic carbon (TOC). The upper and lower portions of the cores are poor in S and a sharp boundary can be traced with the S-rich levels. In the S-poor sections, some S peaks correlate with bromine (Br) and chlorine (Cl). It must be noticed that, on the overall, decreases

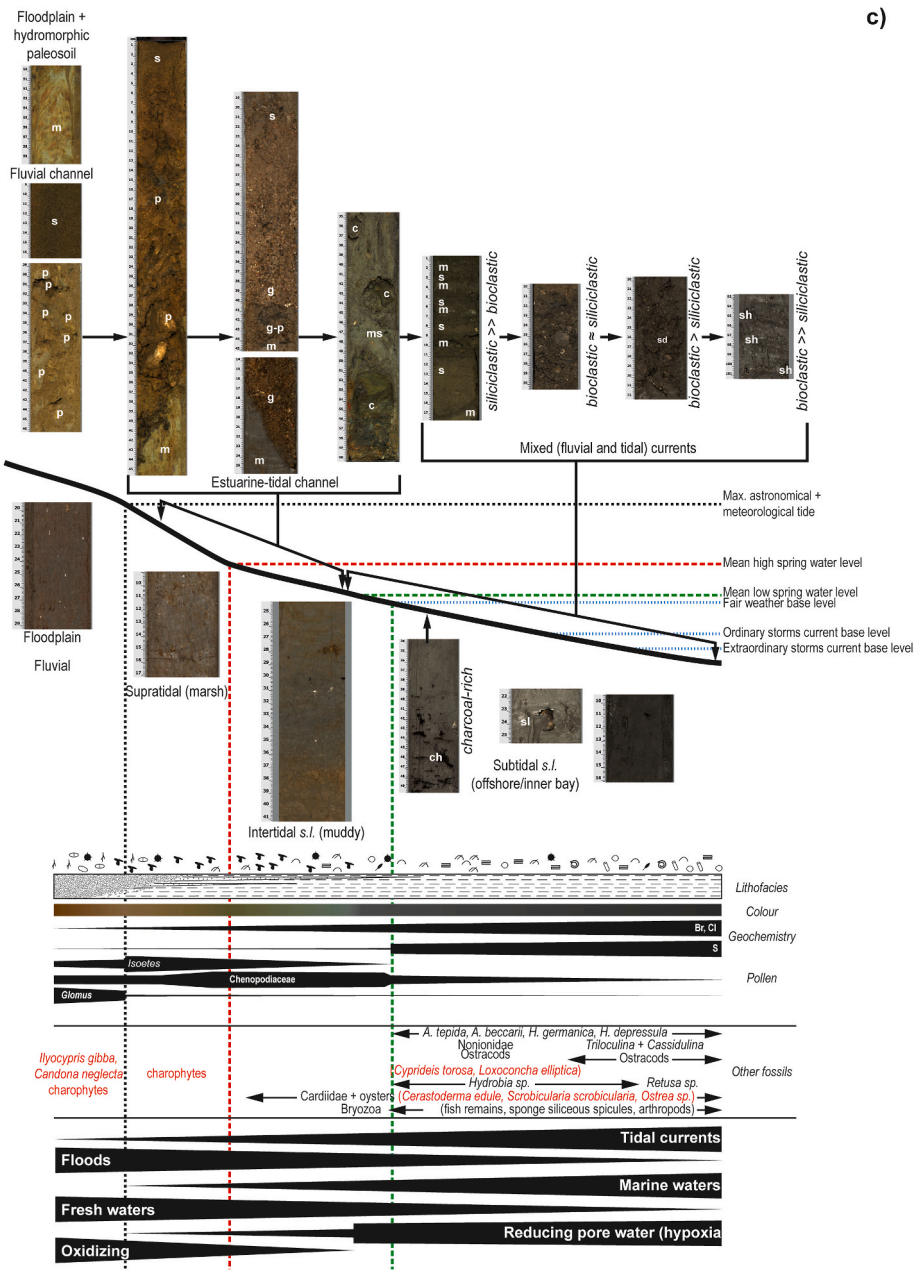

Fig. 3. (*continued*).

in S are correlative to increases in Si or Ca.

Cl and Br variations follow the natrium (Na) and TOC changes, as well as the presence of halite. The lower part of cores S2 and S3 show low contents of Cl and Br, both of which increase somehow abruptly above the transition from the lowermost sands and gravels to the dark muds. This is also noticed in Na and TOC excursions in cores S2 and S3. They show an increasing trend that changes around the middle of the cores S2 and S3 to a decreasing one at the top of the cores. These trends are punctuated by lower content levels that coincide with siliciclastic-rich coarser grain levels.

Br is associated to saline minerals and organic matter (Ziegler et al., 2008) and some authors link the Cl content to pore sea water content (Tjallingii et al., 2007). However, the good correlation to Na data, obtained from dry samples (classical XRF analysis), and to Br and TOC leads us to consider that this content is related to the halite identified by DRX analysis and to the organic matter content. S correlates to pyrite (Chéron et al., 2016). Na and Cl can be absorbed by clay in marine sediments (Charlet and Tournassat, 2005). The fact that Cl and Br do not show a correlation to grain size and that the lower values correspond to the more permeable facies indicates that this is not linked to a present saline aquifer as proposed by Luque et al. (1999).

The correlation of S, Br and Cl with TOC can be indicative of an origin linked to the organic matter, which is common in the case of S. It means that these ions are trapped by the clays and organic matter as the parent minerals are degraded. Thus, we can interpret S as a proxy of reductive conditions (which is also correlated to the preservation of organic matter) while Br and Cl are proxies of sea water influence, as well as of organic content.

3.2.3. Pollen record

The bottom sediments of both cores are characterized by poor preservation of palynomorphs, resulting in low concentrations of all taxa. Samples from core S3 are palynologically sterile for this period and core S2 shows alternating percentages of Chenopodiaceae and *Isoetes*.

Table 2
Radiocarbon data and calibration results for cores JAN-5A, JAN-S2, JAN-S3 and JAN-9A. The rejected samples correspond to possibly reworked material.

Lab code	Number in figures	Sample	Depth in core (m)	^{14}C	error	$\delta^{13}C$	ΔR	error	Cal. BP 2σ Median [range]	Material	Curve
Beta-635182	1	JAN5-1	-2.7	1410	30	-24.5	-	-	1319 [1287–1352]	Organic matter	IntCal20
Beta-635183	2	JAN5-2	-3.9	2010	30	-25.8	-	-	1947 [1869–2002]	Organic matter	IntCal20
Beta-635184	rejected	JAN5-3	-7.7	5840	30	-20.1	-	-	6658 [6596–6739]	Organic matter	IntCal20
Beta-635185	rejected	JAN5-4	-9.7	6520	30	-25.9	-	-	7430 [7418–7505]	Organic matter	IntCal20
UCIAMS-231721	3	JAN-5A	11.5	6625	20		301	201	6580 [6126–7068]	Shell	Marine 20
UCIAMS-236153	rejected	JAN-S2-0	0.46	1100	15		-	-	997 [957–1007]	Charcoal	IntCal20
Beta-618143	4	JAN-S2-1	2.78	1440	30	-20.9	-	-	1331 [1297–1373]	Organic matter	IntCal20
Beta-459036	5	JAN-S2-2	5.16	2480	30	-9.9	-315	220	2353 [1775–2889]	Shell	Marine 20
Beta-459037	6	JAN-S2-4	11.55	6660	30	-2.6	301	201	6618 [6178–7115]	Shell	Marine 20
Beta 459038	7	JAN-S2-5	14.60	7680	30	2.0	301	201	7670 [7260–8093]	Shell	Marine 20
Beta-459039	8	JAN-S2-6	20.44	8220	40	-27.7	-	-	9185 [9024–9302]	Charcoal	IntCal20
Beta-557793	9	JAN-S2-16	23.46	10440	30	-25.0	-	-	12,341 [12,537–12,607]	Charcoal	IntCal20
Beta-635181	10	JANS2-17	26.67	16340	60	-25.0	-	-	19,723 [19,552–19,882]	Organic matter	IntCal20
Beta-526017	11	JAN-S3-2	1.46	400	30	-25.8	-	-	471 [428,512]	Charcoal	IntCal20
Beta-618144	12	JAN-S3-3	4.04	1620	30	-23.2	-	-	1481 [1409, 1544]	Organic matter	IntCal20
Beta-618145	rejected	JAN-S3-4	5.75	2880	30	-26.1	-	-	3008 [2921, 3078]	Organic matter	IntCal20
Beta-526108	13	JAN-S3-5	6.33	2810	30	-25.9	-	-	2912 [2846, 2998]	Charcoal	IntCal20
UCIAMS-259331	14	JAN-S3-6	7.81	4115	15	-5.5	200	426	3744 [2702, 4833]	Shell	Marine 20
Beta-526109	15	JAN-S3-7	8.94	4570	30	-1.6	50	152	4516 [4076, 4925]	Shell	Marine 20
Beta-526110	16	JAN-S3-8	11.23	6760	30	-22.9	-	-	7615 [7574, 7668]	Organic matter	IntCal20
UCIAMS-259332	17	JAN-S3-9	15.51	8040	20	-2.1	17	183	8327 [7911, 8816]	Shell	Marine 20
Beta-526111	18	JAN-S3-10	18.30	7890	30	-26.4	-	-	8668 [8593, 8779]	Vegetal remain	IntCal20
Beta-540083	19	JAN-S3-11	22.64	22400	90	-26.5	-	-	26,728 [26,405–27,006]	Organic matter	IntCal20
UCIAMS-231722	20	JAN-9A 1	5.90	4275	15		-251	169	4523 [4044, 4975]	Shell	Marine 20
UCIAMS-231723	21	JAN-9A 2	11.54	6450	20		301	201	6390 [5920, 6853]	Shell	Marine 20

Thereafter, between ca. 7–10 ka BP in core S2 and ca. 7.5–8.7 ka BP in core S3, the percentages and concentration values of *Isoetes* increase. In both cores, ca. 8–9 ka BP, Chenopodiaceae and *Isoetes* display raised values. Between ca. 3–9 ka BP, Chenopodiaceae progressively increase to the detriment of freshwater vegetation, although displaying variable values and concentration peaks within this period. From ca. 1–3 ka BP, there is an increase in the percentages and concentration values of *Isoetes*, especially remarkable in core S3. There is a peak of Chenopodiaceae ca. 1 ka BP in both cores, which culminates in the decline of both salt marsh and freshwater taxa from this date onwards. On the other hand, *Glomus* concentrations and percentages are rather low in both cores until they undergo a significant rise from ca 1.5 ka to the top of both sections (Val-Peón et al.,).

3.2.4. Other fossil content

The fossil content is low in all the cores. According to Luque et al. (1999), at the top of the section, there are some ostracods (*Ilyiocypris gibba*, *Candona neglecta* and *Candona* sp.) and few charophyte remains, while below 4.5 m in depth occasionally some foraminifera (*Haynesina*, *Ammonia*, *Elphidium*), ostracods (*Cyprideis torosa* and *Loxoconcha elliptica*), bivalves (*Cerastoderma edule*, *Scrobicularia*, and *Ostrea* sp.) and gastropods (*Hydrobia* sp.) are encountered.

We have studied additional samples that allow to include *Retusa* sp., gastropod, few broken remains of bryozoa, fish remains, siliceous spicules of sponges, arthropod remains, and to improve the foraminifera record (*Ammonia tepida*, *A. beccarii*, *Haynesina germanica*, *H. depressula*), as well as a fragment of *Cassidulina*, few small miliolids (*Triloculina*) and possible Nonionidae.

The microfaunal remains are indicative of freshwaters (*Ilyocypris gibba*, *Candona neglecta*, *Candona* sp., charophytes) or brackish waters (*Cyprideis torosa*, *Loxoconcha elliptica*, charophytes, bivalves and gastropods), however a certain marine influence can be deduced from the presence of foraminifera.

3.2.5. Facies and sedimentary model

Four facies groups can be described according to the composition and properties of the sediments and their position in the cores (Fig. 3).

3.2.5.1. Fluvial facies

3.2.5.1.1. Channel subfacies. Ochre to orange siliciclastic sediments

located at the bottom of cores S2 and S3. Poorly to moderately sorted subrounded gravels, sands, and sometimes laminated muds are arranged in fining upward sequences with concave upwards erosive base. The coarsest sediments show internal erosive surfaces. Towards the top of this facies, root traces, mottling and nodules increase typical for a hydromorphic soil.

Sediments show brighter colours and greater density and magnetic susceptibility than the surrounding sediments.

The low calcite content (Ca and TIC) is linked to carbonate clasts derived from the substratum or carbonate nodules. The S content is very low, which correlates with the absence of gypsum and pyrite. Cl and Br content are also low and increase towards the boundary with the supratidal facies.

Sediments are azoic or barren and the pollen content is very low and poorly preserved.

Interpretation: The grain size and erosive base of these deposits are indicative of channelled facies of a certain energy. The presence of internal erosive surfaces reveals that their infill was episodic. The fining upwards sequence, ending with paleosols, indicates filling of these channels sometimes clearly above the ground water table (calcic soils) and others with the ground water table near or at the surface (hydromorphic soils).

3.2.5.1.2. Floodplain/fluvial wetland subfacies. Brown to ochre muds with some sandy layers (in the eastern cores, JAN-03A and JAN-09A) found top section. They show mottling, some charred particles, carbonate nodules and root traces as well as sparse clasts, but with planar boundaries.

They have finer grain sizes and darker tones than their channel equivalents. The coarser levels owe larger magnetic susceptibility and density values than the finer facies.

Their S content is very low and this is linked to the absence of gypsum and pyrite. The calcite, Ca and TIC content is linked to the presence of carbonate nodules and the Br and Cl content is also low but increasing towards the supratidal facies.

The most diagnostic feature is the presence of *Glomus* chlamydospores and the decrease in Chenopodiaceae pollen and *Isoetes* spores, as compared to the underlying levels, as well the presence of *Characeae*. According to Luque et al. (1999), these sediments can contain ostracods (*Ilyiocypris gibba*, *Candona neglecta* and *Candona* sp.) and few charophyte remains.

Interpretation: The colour, finer grain size, planar boundaries and the presence of mottles, nodules and root traces reveal subaerial sedimentation linked to overbanks of the fluvial system. The geochemical features, similar to those of the fluvial channel facies are indicative of clastic supply in a low salinity environment dominated by oxidizing conditions. The abundance of *Glomus*, in comparison of other facies, points to subaerial erosion in a vegetated plain. In addition, the presence of Characeae and freshwater ostracods reveal the development of shallow ephemeral (seasonal?) ponded areas.

3.2.5.2. Supratidal facies. Brown to green muds showing abundant hydromorphic features (mottling), carbonate nodules, organic matter mottles and root traces. A distinctive feature is the presence of some broken shells (bivalves). The hydromorphic features, broken shells and burrowing are more common towards the contact with the intertidal facies and the colour is green. In the proximity of the fluvial facies, root traces and carbonate nodules are more frequent, and the colour is dominantly brown. S, Cl and Br content is low, but larger as the fluvial facies, all along these facies. No gypsum, pyrite or halite have been detected. Ca and TIC are low and related to the presence of carbonate nodules and few shell fragments.

At the base of cores S2 and S3, low concentration and percentages of Chenopodiaceae and *Isoetes* was observed. But towards the top, the percentages and concentration values of all the palynomorphs increase, and few charophytes can be present (Luque et al., 1999). It is remarkable that, at that position, Chenopodiaceae and *Isoetes* show a relative maximum in their percentages.

Interpretation: The fine grain size of these deposits and abundance of edaphic features is interpreted as an area where sedimentation was episodic, probably linked to extreme flood events (marine and fluvial) at the boundary of coastal and fluvial domains. On these mudflats, some stable ponds filled with freshwater (vegetated by *Isoetes*) or brackish waters (surrounded by Chenopodiaceae) developed. The landscape resembles very much present marshes.

3.2.5.3. Intertidal s.l. facies. Mainly green muds changing to ochre towards the boundary with supratidal facies are partly laminated without edaphic features. The muds usually contain shells (broken or unarticulated) and mottles of iron oxides or organic matter and are bioturbated.

Their content in S is low and no gypsum or pyrite have been detected. Cl and Br content is slightly larger than for fluvial and supratidal facies. Some halite is present, but the higher values coincide with organic matter mottles. TIC and Ca (calcite and aragonite) content is low.

Chenopodiaceae pollen show a relative maximum and *Isoetes* an increasing upwards trend while *Glomus* spores percentages are very low.

Interpretation: The dominance of green muds is interpreted as periodic submergence and water saturated pores that sporadically dry (ochre mottles: oxidizing conditions). The abundance of Chenopodiaceae and *Isoetes* are indicative of the presence or proximity to brackish and freshwater ponds. Adding the presence of marine shell fragments and halite, this allows interpreting these deposits as a mudflat in the intertidal area.

3.2.5.4. Subtidal s.l. facies. Dark grey to black muds and clay characterized by the relative abundance of shells in living position and entire unarticulated and broken shells (bivalves and gastropods). They can show parallel lamination, burrowing, organic matter mottles and carbonized vegetal remains (mostly near the boundary with the intertidal facies, where they form conspicuous levels).

In addition to these features, the geochemical and mineralogical composition is more diagnostic. This facies is characterized by the presence of gypsum, pyrite, haematite and halite, and, consequently, the highest content in S, Cl and Br. On the average, these sediments show the highest content in TOC. While the transition to the surrounding intertidal facies is gradual for Br, Cl and TOC, the change in content for S is abrupt, providing a sharp boundary.

It is remarkable that this is the only subfacies in which molluscs in living position have been found, as well as foraminifera, and ostracods change to assemblages with *Cyprideis torosa* and *Loxoconcha elliptica* (Luque et al., 1999). The preservation of pollen and non-palynomorphs is better at the base and decreases to very low values towards the top. *Glomus* is almost absent, Chenopodiaceae is relatively high and *Isoetes* is present at the bottom but nearly disappears towards the top.

Interpretation: The colour, mineralogical, geochemical and fossil composition of this facies point to deposition on a submerged environment and in oxygen-depleted marine waters (hypoxic conditions) The dominance of muddy sediments is typical of an area only sporadically affected by currents. The presence of charcoal-rich levels near the boundary with the intertidal facies are indicative of episodes of riverine input. These conditions correspond to an environment below the fair-weather wave base level and below the low spring tidal level. Thus, this facies can be interpreted as representative of a fair-weather subtidal environment.

3.2.5.5. Estuarine-tidal channel facies. Fining-upwards sequences of gravels to sands, with an erosive base (concave upwards), interbedded with supratidal and intertidal facies. They are composed by siliciclastic, prevailing on supratidal facies, and bioclastic components, more frequent on intertidal facies, that show higher green matrix content and darker tones towards the W. Like the fluvial channel facies, these can

present internal erosive boundaries, but the sediment sorting and roundness increase towards the intertidal facies. They can contain occasionally muddy clasts from the marsh facies and dewatering structures.

Interpretation: Their similarity to the fluvial channel subfacies, position, and increase in hydromorphic features, suggests the extension of the fluvial channels into the supratidal and intertidal areas without discarding a tidal origin for some channels filled with finer-grained sediments.

3.2.5.6. Mixed (fluvial and tidal) current facies. Centimetre to decimetre thick clastic intervals with erosive base ranging from gravel to fine sand have been encountered embedded in intertidal and subtidal facies.

The layers are composed by a mixture of siliciclastic fragments, decreasing content from E to W, and bioclastic fragments, increasing content from E to W. Both fractions show decreasing grain size and increasing matrix content from E to W. The siliciclastic grains are rounded to subangular, they are moderate to well-sorted while the bioclastic fraction is poorly to moderately sorted and scarcely rounded (from entire unarticulated shells to broken fragments). The siliciclastic-dominated layers show lower contents in S, Cl, and Br compared with the muddy facies in which they are included or the bioclastic-dominated levels, and pollen grains are poorly preserved.

Interpretation: The clastic nature of the sediments and their flat erosive base relate them to unconfined currents. The reverse relation between the siliciclastic and S, Br and Cl contents are indicative of an origin linked to freshwater inputs from rivers for this fraction, while the invariance of the geochemical marine proxies for the levels dominated by bioclasts points to marine currents. Wave-related currents are discarded as the dimensions of the basin prevent the formation of waves able to have a noticeable action on the bottom and, thus, tidal currents are invoked for their origin.

Despite both types of currents, fluvial and tidal, would coincide in time, their record at precise times and the wider extension of the bioclastic fraction point to extraordinary tides (astronomical and storm). The westward (seaward) fining of the grain size of both fractions reveals the vanishing of the currents in this sense, and the dominance of ebb vs. flood currents.

3.3. Stratigraphic architecture and paleogeographic evolution

The spatial arrangement and stacking of facies allow to analyse the evolution of the sedimentary system and its main trends in relation with sea level changes (Figs. 4 and 5).

The oldest deposits are fluvial, mainly channelized indicative of a certain slope, lying on an erosive surface carved in the underlying Miocene deposits. These deposits are dated around 27 ka BP in core S3 and ca. 20 ka BP in core S2, where they are encountered around 3 m deeper than in core S3. This arrangement points to a staircase disposition of the fluvial facies that is compatible with a sea level drop of near 11 m in ca. 4 ka, according to the sea level model of Lambeck et al. (2014). These features, coherent with a forced regression, along with the development of a hydromorphic soil on top of the deposits allow to interpret the S3 deposits as sedimented during a sea level fall in the falling stage systems tract (FSST after Catuneanu et al., 2011; Catuneanu, 2019). While those of core S2 have been accumulated during the beginning of the rise in the lowstand systems tract (LST) (after Catuneanu et al., 2011; Catuneanu, 2019). For this period sedimentation rates were below 1 mm/yr.

The beginning of the transgression (transgressive systems tract, TST) is evidenced by the above mentioned paleosol, marking the transgressive surface (ts), and the development of supratidal facies, ca. 12–17 ka BP in core S2 and ca. 10–11 ka BP in core S3, and intertidal, ca. 10–12 ka BP in core S2 and ca. 8.7–10 ka BP in core S3. The marine water incursion reached the location of core S2 around 10 ka BP, causing the development of hypoxic conditions. The continued sea level rise caused the marine flooding of higher areas (core S3) around 8.7 ka BP. During this transgressive period, in the inner bay areas, only bioclastic ebb current-related deposits are found in cores S2 and S3 but no siliciclastic or mixed deposits (fluvial or fluvial and tidal current), probably recording the fast landward shifting of the river mouths.

In the meantime, coarse grain deposits accumulated in the supra- and intertidal areas. This can be explained due to a fast sea level rise upon a steep slope of a narrow palaeovalley, so channelized facies prevail, and

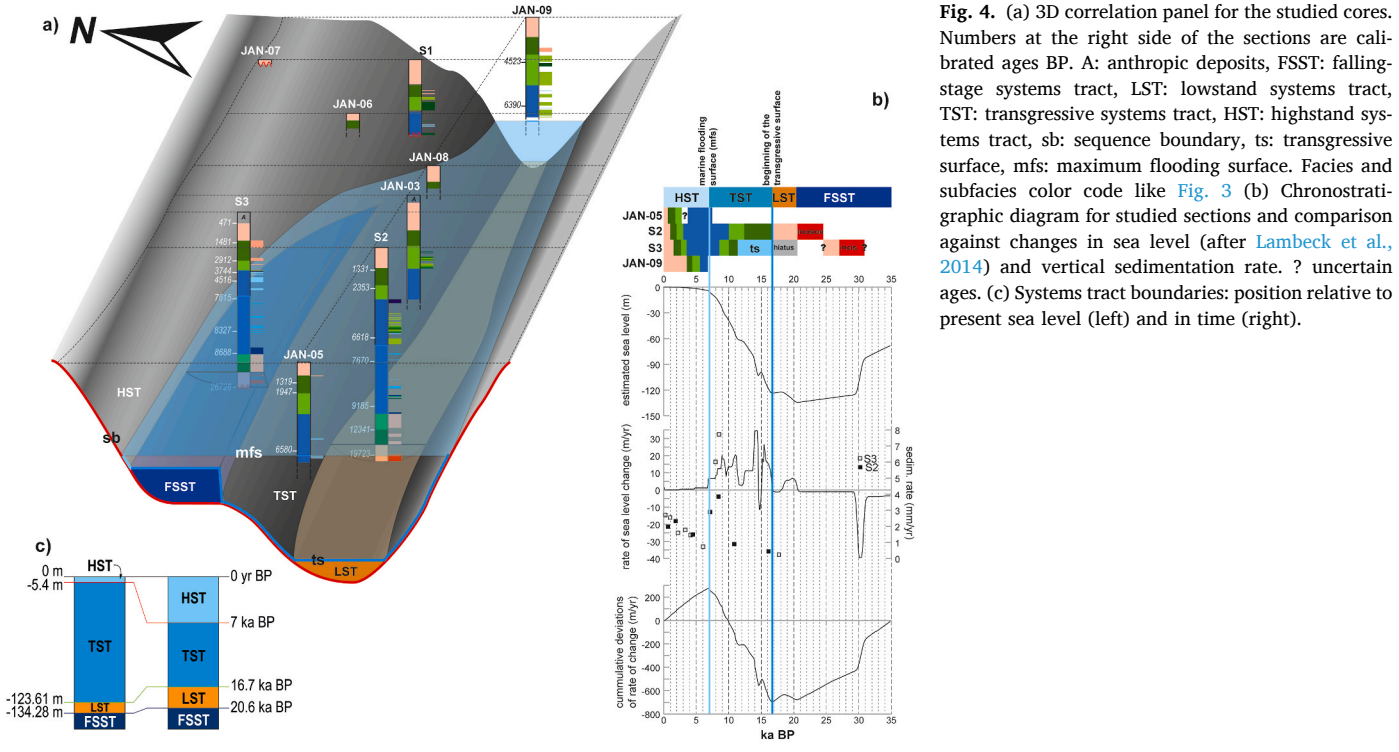

Fig. 4. (a) 3D correlation panel for the studied cores. Numbers at the right side of the sections are calibrated ages BP. A: anthropic deposits, FSST: falling-stage systems tract, LST: lowstand systems tract, TST: transgressive systems tract, HST: highstand systems tract, sb: sequence boundary, ts: transgressive surface, mfs: maximum flooding surface. Facies and subfacies color code like Fig. 3 (b) Chronostratigraphic diagram for studied sections and comparison against changes in sea level (after Lambeck et al., 2014) and vertical sedimentation rate. ? uncertain ages. (c) Systems tract boundaries: position relative to present sea level (left) and in time (right).

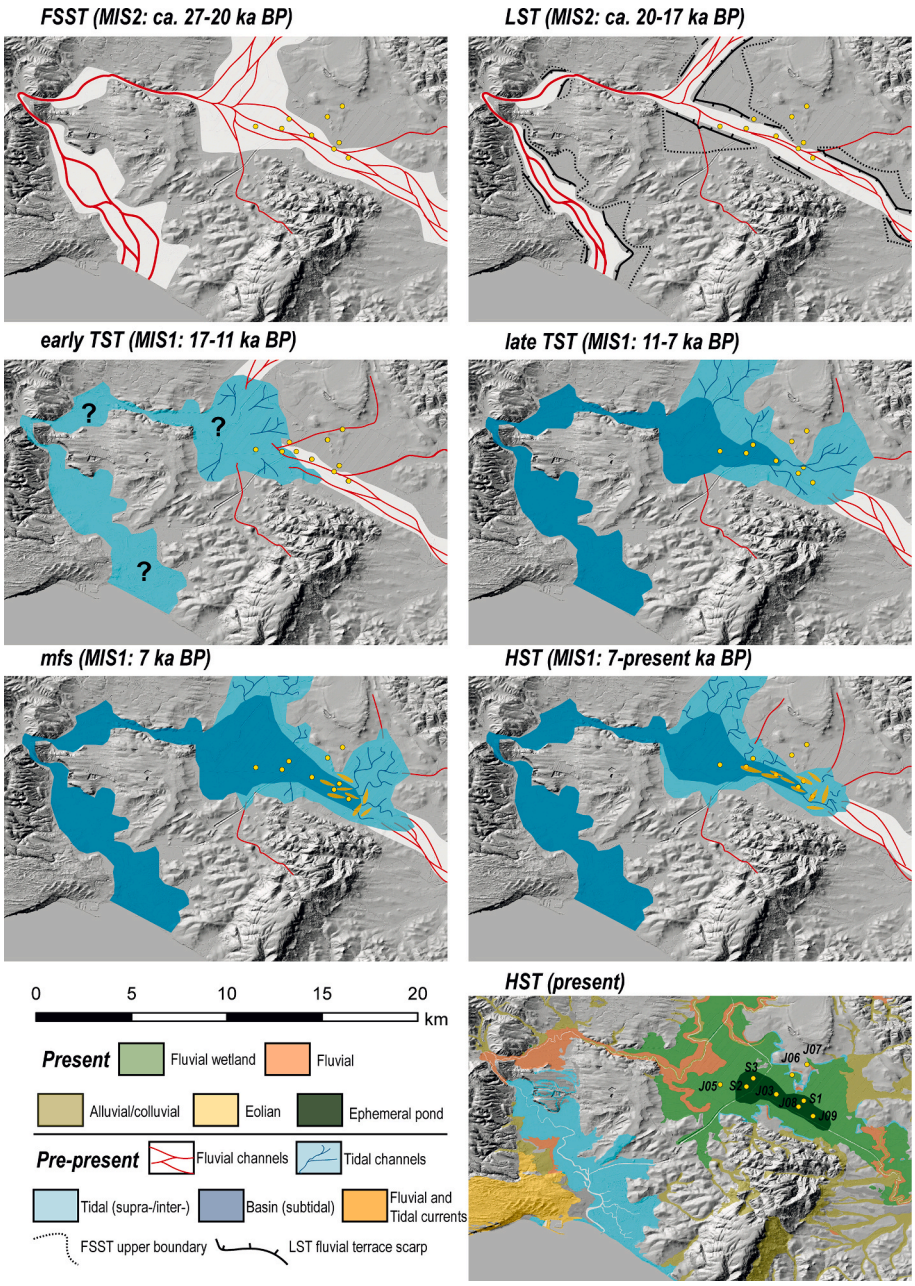

Fig. 5. Paleogeographic reconstruction for the last 27 ka BP.

older fluvial sediments were easily reworked in the coastal areas as the coastline retreated landwards. This is confirmed by the sudden change to fine grain subtidal deposits and low sedimentation rates (≈1 mm/yr), implying a fast transgression. During the last stage of the TST to ca. 9 ka BP, sedimentation rates showed a noticeable increase up to 8 mm/yr for core S3, and 4 mm/yr for core S2, that could be related to more sediment availability and increased accommodation space.

The marine maximum flooding surface (mfs) is marked by a fall in the sedimentation rate down to ca. 1 mm/yr and a change in the stacking pattern, from aggradation with retrogradation to progradation, that took place around 7 ka BP.

After 7 ka BP, sea level rise began to slow down and changes in sedimentation took place. Fluvial or tidal current deposits were more abundant in time and space, except for core S3 where they are absent and ebb current deposits are more frequent. In addition, sedimentation rates increased to 2–3 mm/yr. The change to a progradational, normal regression, and the rise of sedimentation rates imply a change in the sedimentation/accommodation rate, in favour of the first, and the beginning of the highstand systems tract (HST).

The increase in sedimentation rate and decrease of sea level rise caused the advance of coastal and terrestrial systems, near river mouth areas, fluvial or tidal current structures advanced into the estuary of the Almodóvar River (cores JAN-09, S1, JAN-03, S2). On the other hand, the decrease of slope/gradient due to the basin infill, promoted the accumulation of finer sediments in comparison to channelized facies and increased the surface affected by tidal currents that were recorded in those areas far from river mouths (core S3).

At the present stage of the HST, the progradation of the terrestrial systems has transformed the area in an episodically ponded fluvial plain (Fig. 5).

4. Discussion

In the Gulf of Cádiz, several sedimentological, paleontological and

geochemical studies focused on the recent dynamics of its estuaries and their facies (Dabrio, 1982; Borrego et al., 1995, 2004; Ruiz et al., 2004; Morales et al., 2006). However, few of these records are long enough and well-dated as to obtain a reliable correlation among them. In this section, the records of the La Janda wetland of the Almodóvar estuary (this study), the Guadalete and Odiel-Tinto (Dabrio et al., 1999, 2000), the Guadiana (Boski et al., 2008) and the Quarteira (Schneider et al., 2010) estuaries are compared (Fig. 6).

All the records are found in incised valleys, carved into a Neogene (La Janda, below −23 m a.s.l., and Odiel-Tinto, −35 m a.s.l.) or Paleozoic (Guadiana, −51 m a.s.l.) substratum, and start with a basal fluvial unit.

In the Odiel-Tinto area, this fluvial unit has only been dated in core SN11 as 25–30 ka BP (Dabrio et al., 1999), and this age was assumed for the whole unit for the Guadalete and Guadiana areas (Dabrio et al., 2000; Boski et al., 2008). This single dated interval prevented the identification of any stratigraphic architecture for this unit and, using previous time scales, placed it on Isotopic Stage 3, during a previous highstand (HST) that did not reach present sea level. Consequently, the erosive surface at top of this unit recorded the LST of the last stratigraphic sequence, and it was its boundary (Dabrio et al., 1999, 2000).

There are no reliable dates for the fluvial unit at the base of the Quarteira record, but they have been attributed to 7.5–8 ka BP, a pre-transgressive period as they assume that the transgression started at about 7.5 ka BP (Schneider et al., 2010).

In La Janda area, the fluvial unit has provided ages of 27 ka BP (core S3) and 20 ka BP (core S2) and shows a staircase disposition in a riverine environment.

New time scales and sea level reconstructions and models (Lisiecki and Raymo, 2005; Lambeck et al., 2014; Spratt and Lisiecki, 2016; Past Interglacials WG Past Interglacials Working Group of PAGES, 2016) place the MIS 3/2 boundary at 29 ka BP and consider that the MIS 3 was not a true highstand (Fig. 6a). Recalibrated dates of Odiel-Tinto area are between 29 and 30 ka BP, and these and La Janda dates encompass the end of a sea level fall period, according to the sea level reconstruction of Lambeck et al. (2014) (Fig. 6). Consequently, the fluvial sediments dated between 27 and 30 ka BP and the erosive surface below and the following fluvial deposits accumulated during the FSST (Fig. 6b and c). The La Janda fluvial sediments dated as ca. 20 ka BP are affected by a

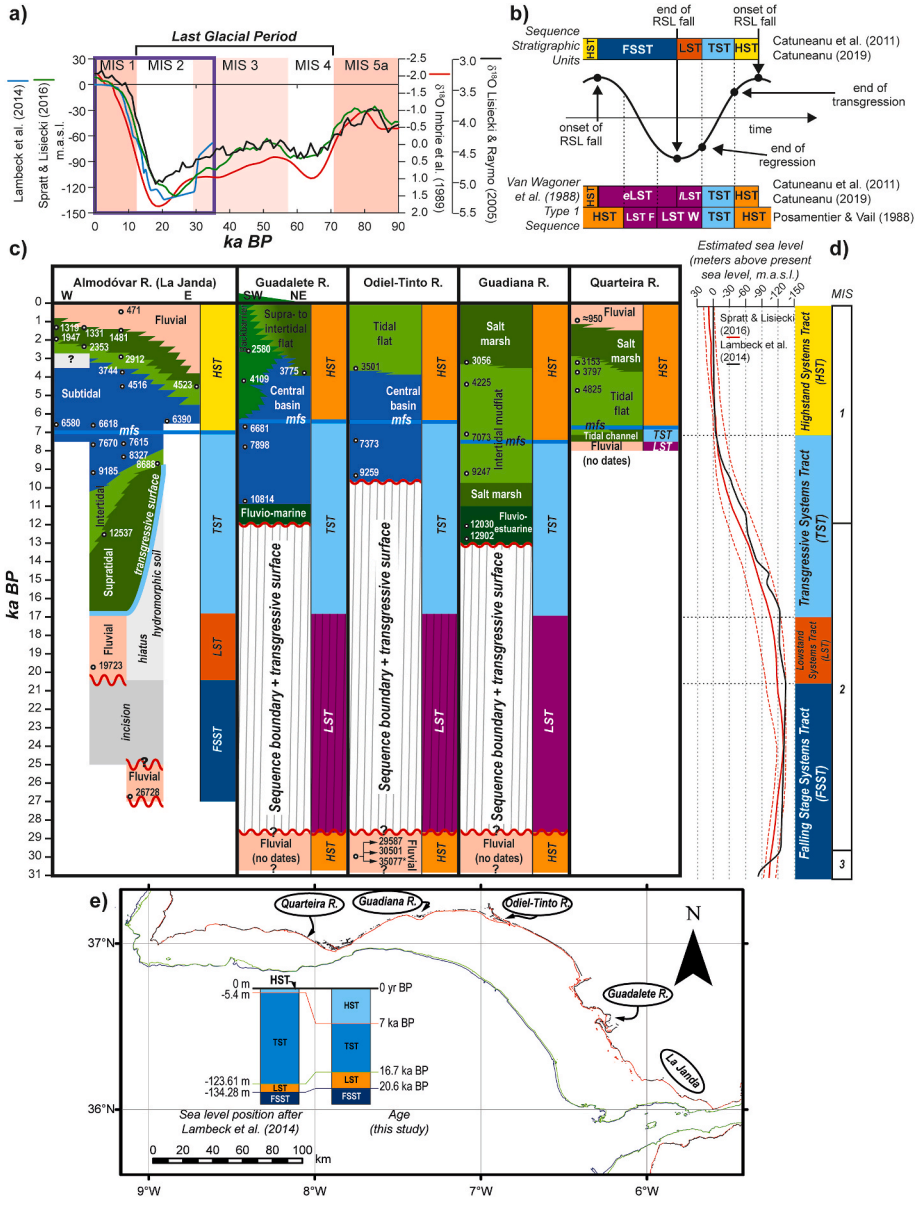

Fig. 6. (a) Chronological placement of the studied period (purple square), sea level curves (Lambeck et al., 2014; Spratt and Lisiecki, 2016) and oxygen isotope reference curves (SPECMAP: Imbrie et al. (1989); LR04: Lisiecki and Raymo (2005). Marine Isotope Stages (MIS) after Lisiecki and Raymo (2005) except for the MIS 2/1 boundary that has been placed in the more accepted value of 11.7 ka BP. (b) Conceptual model relating Van Wagoner et al. (1988) type 1 sequence systems tracts (after Posamentier and Vail, 1988, and Catuneanu et al., 2011, 2019) and Catuneanu et al. (2011) systems tracts. FSST: falling stage systems tract, LST: lowstand systems tract, eLST: early LST, LST F: LST fan, lLST: late LST, LST W: LST wedge, TST: transgressive systems tract, HST: highstand systems tract. (c) Comparison of the Late Pleistocene-Holocene record of five estuarine areas in SW Iberian Peninsula: La Janda (this work), Guadalete River (Dabrio et al., 2000), Odiel-Tinto rivers (Dabrio et al., 2000), Guadiana River (Boski et al., 2008), Quarteira River (Schneider et al., 2010). All the dates have been recalibrated by using IntCal20 and Marine20 curves (the date marked with an * should be discarded as it can be reworked, but it has been included because the original authors did it). (d) Proposal of stratigraphic architecture for the Gulf of Cádiz: sea level data from Lambeck et al. (2014) model and Spratt and Lisiecki (2016) reconstruction, systems tracts, and MIS. (e) Location of the compared estuaries and the inferred position of the coastline for the end of each systems tract. Bathymetric data from EMODNET (EMODNET, 2020).

hydromorphic paleosol, piled up at lower topographic positions during the beginning of the last sea level rise and, therefore, represent the LST (Fig. 6b and c). We cannot rule out that part of the undated sediments of the Guadalete, Odiel-Tinto, Guadiana and Quarteira areas could be included in any of these system tracts.

Marine flooding was diachronous and its beginning was recorded at different moments in each estuary. Thus, in the Almodovar estuary (La Janda) the first record is ca. 16.7 ka BP, in the Guadalete before 10.5 ka BP, in the Odiel-Tinto around 10 ka BP, in the Quarteira estuary ca. 7.5 ka BP and in the Guadiana River around 13 ka BP.

From this time on until the maximum marine flooding, ca. 7 ka BP, the sediments show a transgressive pattern that in the open Almodóvar, Quarteira and Guadiana estuaries is recorded by a supratidal, intertidal to estuarine basin or salt marsh to mud flat. The Guadalete estuary was protected by the rocky substratum that bounds the Cádiz Bay and the TST record is composed by fluvio-marine (head bay delta) to estuarine basin, with flood delta deposits (Dabrio et al., 2000) what supports the hypothesis of a confined estuary.

The position of the mfs in time and depth is variable among estuaries (La Janda: 7 ka BP, 10.8–12.7 m b.s.; Guadalete: 6.5 ka BP, 10.5 m b.s.; Odiel-Tinto: 6.5 ka BP, 14.3 m b.s.; Guadiana: 7.5 ka BP, 9.4 m b.s.; Quarteira: 6.7 ka BP, 6.0 m b.s.) accordingly to the different studies. And the position of the arbitrary 7 ka BP reference level, at 10.8–12.7 m b.s. (La Janda), 13.3 m b.s. (Guadalete), 17.0 m b.s. (Odiel-Tinto), 9.0 m b.s. (Guadiana), and 6.9 m b.s. (Quarteira), point to tectonic activity as modifying these records.

After 7 ka BP, the rate of sea level rise slows down (HST) and this is invoked as the trigger of the development of barrier islands (Freitas et al., 2003). The barrier island systems developed in the Guadalete estuary until ca. 3 ka BP, when they change to spit systems and intertidal and supratidal deposits. In the Guadiana estuary, the barrier island systems established at marine positions (5640–6250 yrs BP, Boski et al., 2002) while, upstream, intertidal systems, evolving to salt marshes, filled the valley.

In the Odiel-Tinto estuary, the HST was composed of central basin and sand shoals evolving to tidal flats. This was an open estuary that began to close around 3 ka BP as the present spit systems started to grow.

The HST of the open estuaries of Quarteira and Almodóvar are very similar, and they record the infill of the estuarine basin. In Quarteira, tidal channels and tidal flats developed until ca. 4.1 ka BP, when the sea influence clearly vanished and salt marshes changing into fluvial floodplains prevailed. In the Almodóvar estuary (La Janda), the inner bay and mixed current deposits were gradually substituted by intertidal, supratidal and fluvial floodplain that were episodically ponded.

The clogging of the estuaries can be better explained by the destruction of accommodation space by infilling, whereas the formation of the spit systems played a minor control. In all examples the fluvial systems advance on the estuarine areas, but the present stage of this change is variable.

5. Conclusions

The multiproxy approach combining sedimentological, geochemical, palynological and paleontological data to study the sedimentary record of the last 26,000 years of La Janda wetland enables a detailed characterization of facies by the interpretation of the complementary proxies. Using a robust age-depth model and a 3D reconstruction of the stratigraphic architecture of the deposits, we conclude that these sediments record the infill of an incised valley carved during the last sea level fall.

As a peculiarity, the location of the system inside a restricted valley, bounded by rocky hills, and with a narrow connection to the open sea caused that the dynamics of the environment was conditioned by the topography, slope gradient, erosion rates and by the basin infill.

The sediments corresponding to the FSST (older than 20.6 ka BP) and LST (16.7–20.6 ka BP) are first identified in this area for the Gulf of Cádiz.

The scarcity of dates for these sediments in other areas around the Gulf of Cádiz prevents the clear identification of the system tracts in a sequence stratigraphic interpretation as previous studies placed them in the MIS 3, and assumed a highstand, which led to the interpretation as belonging to an older sequence (Fig. 6).

Around the Gulf of Cádiz, the evolution of the TST and HST was controlled by the morphology of the estuaries (open, Odiel-Tinto, narrow at its mouth, Guadiana, narrow during the whole valley, Quarteira), the rocky substratum that protects the estuaries from the sea action (Guadalete and Almodóvar), and tectonic activity, as the main reference levels (i.e. maximum marine flooding surface) are found today at different depths among estuaries. These differences can be observed in the regressive and transgressive stages, but they are more noticeable in the latter.

During the TST (16.7–7 ka BP), all estuaries experienced a fast deepening from supratidal to estuarine basin environments and the widening of the valleys.

The maximum extent of the marine flooding was reached around the Gulf of Cádiz ca. 7 ka BP. Afterthat, the sea level rise rate slowed down in addition to a widening of the paleovalleys and decreasing slopes by erosion and infilling of the basin, which promoted the normal regression of the HST sediments (7 ka BP to present). The period is characterized by a marine basin and estuarine conditions dominated by tides. During final stages of the HST, the basin was occupied by a ponded fluvial floodplain that constitutes present landscape for the Quarteira and Almodóvar estuaries while tidal flats and salt marshes developed in the Guadalete, Odiel-Tinto and Guadiana estuaries.

As a conclusion, the incised valleys of the Campo de Gibraltar region developed under the identical climate and sea level conditions. Therefore, their differences must be linked to allocyclic controls, mainly basin morphology and composition that, in turn, control the estuarine hydrodynamics (waves, tidal currents and fluvial supplies) and the amount of sediment available from marine sources, and active tectonics.

A better knowledge of the reaction of these systems under such climate and tectonic variability is a key to evaluate their future evolution under the changing climate scenarios.

Author's contributions

Rosa Mediavilla: Conceptualization; Data curation; Funding acquisition; Investigation; Methodology; Project administration; Supervision; Visualization; Writing - original draft. Juan I. Santisteban: Conceptualization; Data curation; Formal Analysis; Investigation; Methodology; Supervision; Visualization; Writing - original draft. Cristina Val-Peón: Data curation; Investigation; Writing - original draft. Luis Galán de Frutos: Data curation; Resources; Writing – review and editing. Margret Mathes-Schmidt: Data curation; Investigation; Writing - review and editing. José Antonio López-Sáez: Investigation; Writing - review and editing. Francisco J. Gracia: Investigation; Writing - review and editing. Klaus Reicherter: Funding acquisition; Investigation; Project administration; Writing - review and editing.

Declaration of competing interest

The authors declare the following financial interests/personal relationships which may be considered as potential competing interests:

Klaus Reicherter reports financial support was provided by Deutsche Forschungsgemeinschaft.

Rosa Mediavilla reports financial support was provided by Spain Ministry of Science and Innovation.

Acknowledgements

The authors are grateful to the "Centro Nacional IGME, CSIC" for the analytical facilities provided for this study. We are also in debt to the

colleagues from the U. Köln and RWTH-Aachen for all the support in the field. This research was funded by the Deutsche Forschungsgemeinschaft (DFG project no.57444011 – SFB 806) and a "Severo Ochoa" extraordinary grant for excellence IGME-CSIC (AECEX2021). The authors are grateful to the CEOs, managers and personnel of "Las Lomas" farm for all their help during the drilling and in the accurate positioning of the drilling points.

References

Allard, J., Chaumillon, E., Bertin, X., Poirier, C., Ganthy, F., 2010. Sedimentary record of environmental changes and human interferences in a macrotidal bay for the last millenaries: the Marennes-Oléron Bay (SW France). Bull. Soc. Geol. Fr. 181, 151–169. https://doi.org/10.2113/gssgfbull.181.2.151.

Allen, G.P., Posamentier, H.W., 1994. Transgressive facies and sequence architecture in mixed tide-and wave-dominated incised valleys: example from the Gironde estuary, France. In: Dalrymple, R.W., Boyd, R., Zaitlin, B.A. (Eds.), Incised-valleys Systems: Origin and Sedimentary Sequences, vol. 51. SEPM Special Publication, pp. 225–240. https://doi.org/10.2110/pec.94.12.0225.

Anderson, R.S., Homola, R.L., Davis, R.B., Jacobson Jr., G.L., 1984. Fossil remains of the mycorrhizal fungal *Glomus fasciculatum* complex in postglacial lake sediments from Maine. Can. J. Bot. 62, 2325–2328. https://doi.org/10.1139/b84-316.

Anderson, R.S., Jiménez-Moreno, G., Carrión, J.S., Pérez-Martínez, C., 2011. Postglacial history of alpine vegetation, fire, and climate from Laguna de Río Seco, Sierra Nevada, southern Spain. Quat. Sci. Rev. 30, 1615–1629. https://doi.org/10.1016/j.quascirev.2011.03.005.

Azañón, J.M., Galindo-Zaldívar, J., García-Dueñas, V., Jabaloy, A., 2002. Alpine tectonics II: betic cordillera and balearic islands. In: Gibbons, W., Moreno, T. (Eds.), The Geology of Spain. Geological Society of London, Geology of Series, pp. 401–416. https://doi.org/10.1144/GOSPP.16.

Balnayá, J.C., García Dueñas, V., 1988. Les directions structurales dans le Domaine d'Alborán de part et d'autre du Détroit de Gibraltar. Comptes rendus de l'Académie des sciences. Série 2, Mécanique, Physique, Chimie, Sciences de l'univers, Sciences de la Terre 304, 929–932.

Benkhelil, J., 1976. Étude Tectonique de la Terminaison Occidentale des Cordillères Bétiques (Espagne). Ph.D. Thesis. Univ. Nice, p. 180.

Billeaud, I., Tessier, B., Lesueur, P., 2009. Impacts of late Holocene rapid climate changes as recorded in a macrotidal coastal setting (Mont-Saint-Michel Bay, France). Geology 37, 1031–1034. https://doi.org/10.1130/G30310A.1.

Blaauw, M., 2022. Clam: classical age-depth modelling of cores from deposits. R package version 2.5.0. https://CRAN.R-project.org/package=clam.

Blaauw, M., Christen, J.A., 2011. Flexible paleoclimate age-depth models using an autoregressive gamma process. Bayesian Analysis 6 (3), 457–474. https://doi.org/10.1214/11-BA618.

Borrego, J., Morales, J.A., Pendón, J.G., 1993. Holocene filling of an estuarine lagoon along the mesotidal Coast of Huelva: the Piedras River mouth, southwestern Spain. J. Coast Res. 8, 321–343.

Borrego, J., Morales, J.A., Pendón, J.G., 1995. Holocene estuarine facies along the mesotidal coast of Huelva, south-western Spain. In: Flemming, B.W., Bartholomä, A. (Eds.), Tidal Signatures in Modern and Ancient Sediments, vol. 24. International Association of Sedimentologists Special Publication, pp. 151–170. https://doi.org/10.1002/9781444304138.ch10.

Borrego, J., Ruiz, F., González-Regalado, M.L., Pendón, J.G., Morales, J.A., 1999. The Holocene transgression into the estuarine basin of the Odiel River mouth (Cadiz Gulf, SW Spain): lithology and faunal assemblages. Quat. Sci. Rev. 18, 769–788. https://doi.org/10.1016/S0277-3791(97)00085-1.

Borrego, J., López González, N., Carro, B., 2004. Geochemical signature as paleoenvironmental markers in Holocene sediments of the Tinto River estuary (Southwestern Spain). Estuar. Coast Shelf Sci. 61, 631–641. https://doi.org/10.1016/j.ecss.2004.07.004.

Boski, T., Moura, D., Camacho, S., Duarte, R.D.N., Scott, D.B., Veiga Pires, C., Pedro, P., Santana, P., 2002. Postglacial sea level rise and sedimentary response in the Guadiana Estuary, Portugal/Spain border. Sediment. Geol. 150, 103–121. https://doi.org/10.1016/S0037-0738(01)00270-6.

Boski, T., Camacho, S., Moura, D., Fletcher, W., Wilamowski, A., Veiga-Pires, C., Correia, V., Loureiro, C., Santana, P., 2008. Chronology of the sedimentary processes during the postglacial sea level rise in two estuaries of the Algarve coast, Southern Portugal. Estuar. Coast Shelf Sci. 77, 230–244. https://doi.org/10.1016/j.ecss.2007.09.012.

Boyd, R., Dalrymple, R.W., Zaitlin, B.A., 2006. Estuarine and incised-valley facies models. In: Posamentier, H.W., Walker, R.G. (Eds.), Facies Models Revisited, vol. 84. SEPM Special Publication, pp. 171–235. https://doi.org/10.2110/pec.06.84.0171.

Catuneanu, O., 2019. Model-independent sequence stratigraphy. Earth Sci. Rev. 188, 312–388. https://doi.org/10.1016/j.earscirev.2018.09.017.

Catuneanu, O., Galloway, W.E., Kendall, C.G.StC., Miall, A.D., Posamentier, H.W., Strasser, A., Tucker, M.E., 2011. Sequence stratigraphy: methodology and nomenclature. Newsl. Stratigr. 44, 173–245. https://doi.org/10.1127/0078-0421/2011/0011.

Cearreta, A., Irabien, M.J., Pascual, A., 2004. Human activities along the Basque coast during the last two centuries: geological perspective of recent anthropogenic impact on the coast and its environmental consequences. In: Borja, A., Collins, M. (Eds.), Oceanography and Marine Environment of the Basque Country, vol. 70. Elsevier Oceanography Series, pp. 27–50. https://doi.org/10.1016/S0422-9894(04)80040-0.

Cearreta, A., García-Artola, A., Leorri, E., Irabien, M.J., Masque, P., 2013. Recent environmental evolution of regenerated salt marshes in the southern Bay of Biscay: anthropogenic evidences in their sedimentary record. J. Mar. Syst. 109–110, S203–S212. https://doi.org/10.1016/j.jmarsys.2011.07.013.

Charlet, L., Tournassat, C., 2005. Fe(II)–Na(I)–Ca(II) cation exchange on montmorillonite in chloride medium: evidence for preferential clay adsorption of chloride – metal ion pairs in seawater. Aquat. Geochem. 11, 115–137. https://doi.org/10.1007/s10498-004-1166-5.

Chaumillon, E., Proust, J.N., Menier, D., Weber, N., 2008. Incised-valley morphologies and sedimentary-fills within the inner shelf of the Bay of Biscay (France): a synthesis. J. Mar. Syst. 72, 383–396. https://doi.org/10.1016/j.jmarsys.2007.05.014.

Chéron, S., Etoubleau, J., Bayon, G., Garziglia, S., Boissier, A., 2016. Focus on sulfur count rates along marine sediment cores acquired by XRF Core Scanner. X Ray Spectrom. 45, 288–298. https://doi.org/10.1002/xrs.2704.

Cirujano, S., Meco, A., Garcia Murillo, P., 2014. Flora Acuática Española. Hidrófitos Vasculares. Real Jardín Botánico, CSIC, Madrid, p. 320. https://bibdigital.rjb.csic.es/medias/de/8d/6e/e0/de8d6ee0-a308-48e7-afd9-4cb883a336d5/files/CIR_Fl_Acu_Esp_Hidro_Vasc.pdf.

Crema, E.R., Bevan, A., 2021. Inference from large sets of radiocarbon dates: software and methods. Radiocarbon 63, 23–39. https://doi.org/10.1017/RDC.2020.95.

Dabrio, C.J., 1982. Sedimentary structures generated on the foreshore by migrating ridge and runnel systems on microtidal and mesotidal coast on S. Spain. Sediment. Geol. 32, 141–151. https://doi.org/10.1016/0037-0738(82)90018-5.

Dabrio, C.J., Zazo, C., Lario, J., Goy, J.L., Sierro, F.J., Borja, F., González, J.A., Flores, J. A., 1999. Sequence stratigraphy of Holocene incised-valley fills and coastal evolution in the Gulf of Cadiz southern Spain. Geol. Mijnbouw 77, 263–281. https://doi.org/10.1023/A:1003643006015.

Dabrio, C.J., Zazo, C., Goy, J.L., Sierro, F.J., Borja, F., Lario, J., González, J.A., Flores, J. A., 2000. Depositional history of estuarine infill during the last postglacial transgression (Gulf of Cadiz, southern Spain). Mar. Geol. 162, 381–404. https://doi.org/10.1016/S0025-3227(99)00069-9.

Dalrymple, R.W., Boyd, R., Zaitlin, B.A., 1994. History of research, types and internal organisation of incised valley systems: introduction to the volume. In: Dalrymple, R. W., Boyd, R., Zaitlin, B.A. (Eds.), Incised-Valley Systems: Origin and Sedimentary Sequences, vol. 51. SEPM Special Publication, pp. 225–240. https://doi.org/10.2110/pec.94.12.0003.

de Castro, S., Lobo, F.J., 2018. Sedimentary infilling of bedrock-controlled palaeo-embayments off Cape trafalgar, strait of Gibraltar (Gulf of Cadiz). Geo Mar. Lett. 38, 47–62. https://doi.org/10.1007/s00367-017-0508-4.

Domínguez, E., Blanca, G., Valdés, B., Cabezudo, B., Nieto, J.M., Silvestre, S., 1993. Introducción a la flora andaluza. Agencia del Medio Ambiente, Sevilla, p. 79, 84-87294-40-5.

Dueñas López, M.A., Recio Espejo, J.M., 2000. Bases ecológicas para la restauración de los humedales de La Janda (Cádiz, España). Universidad de Córdoba, Córdoba, Spain, p. 476.

Dunlea, A.G., Murray, R.W., Tada, R., Alvarez-Zarikian, C.A., Anderson, C.H., Gilli, A., Giosan, L., Gorgas, T., Hennekam, R., Irino, T., Murayama, M., Peterson, L.C., Reichart, G.-J., Seki, A., Zheng, H., Ziegler, M., 2020. Intercomparison of XRF core scanning results from seven labs and approaches to practical calibration. G-cubed 21, e2020GC009248. https://doi.org/10.1029/2020GC009248.

EMODNET, 2020. EMODNET bathymetry (DTM) 2020, 15/01/2023. https://emodnet.ec.europa.eu/en/bathymetry.

Evans, G., 2008. Man's impact on the coastline. J. Iber. Geol. 34, 167–190.

Freitas, M.C., Andrade, C., Rocha, F., Tassinari, C., Munhá, J.M., Cruves, A., Vidinha, J., Marques da Silva, C., 2003. Lateglacial and Holocene environmental changes in Portuguese coastal lagoons 1: the sedimentological and geochemical records of the Santo André coastal area. Holocene 13, 433–446. https://doi.org/10.1191/0959683603hl636rp.

Galán de Mera, A., Vicente Orellana, J., Sánchez, I., 1997. Coastal plant communities of the southwestern Iberian Peninsula, Spain and Portugal. Phytocoenologia 27, 313–352. https://doi.org/10.1127/phyto/27/1997/313.

García de Domingo, A., González-Lastras, J., Hernaiz Huerta, P.P., Zazo Cerdeña, C., Goy Goy, J.L., 1991. *Cartografía geológica y memoria de la hoja 12–47/12-48 (Vejer de la Frontera)*. Mapa Geológico de España, Escala 1:50.000. Plan MAGNA, 2ª Serie, Madrid, Spain, p. 43. IGME.

González-Castillo, L., Galindo-Zaldívar, J., Junge, A., Martínez-Moreno, F.J., Löwer, A., de Galdeano, C.S., Pedrera, A., López-Garrido, A.C., Ruiz-Constán, A., Ruano, P., Martínez-Martos, M., 2015. Evidence of a large deep conductive body within the basement of the Guadalquivir foreland Basin (Betic Cordillera, S-Spain) from tipper vector modelling: tectonic implications. Tectonophysics 663, 354–363. https://doi.org/10.1016/j.tecto.2015.08.013.

Goy, J.L., Zazo, C., Silva, P.G., Lario, J., Bardají, T., Somoza, L., 1995. Evaluación geomorfológica del comportamiento neotectónico del Estrecho de Gibraltar (Zona Norte) durante el Cuaternario. In: Esteras, M. (Ed.), El Enlace Fijo del Estrecho de Gibraltar, vol. 2. SECEGSA, Madrid, pp. 51–69.

Gracia, F.J., Rodríguez-Vidal, J., Benavente, J., Cáceres, L., López-Aguayo, F., 1999. Tectónica Cuaternaria en la Bahía de Cádiz. In: Pallí, L., Roque, C. (Eds.), Avances en el estudio del Cuaternario español. AEQUA-UdG, Girona, Spain, pp. 67–74.

Haasnoot, M., Winter, G., Brown, S., Dawson, R.J., Ward, P.J., Eilander, D., 2021. Long-term sea-level rise necessitates a commitment to adaptation: a first order assessment. Climate Risk Management 34, 100355. https://doi.org/10.1016/j.crm.2021.100355.

Haslett, J., Parnell, A.C., 2008. A simple monotone process with application to radiocarbon-dated depth chronologies. J. Roy. Stat. Soc.: Series C (Applied Statistics) 57, 399–418. https://doi.org/10.1111/j.1467-9876.2008.00623.x.

Heaton, T.J., Köhler, P., Butzin, M., Bard, E., Reimer, R.W., Austin, W.E.N., Bronk Ramsey, C., Grootes, P.M., Hughen, K.A., Kromer, B., Reimer, P.J., Adkins, J., Burke, A., Cook, M.S., Olsen, J., Skinner, L.C., 2020. Marine20 - the marine radiocarbon age calibration curve (0-55,000 cal BP). Radiocarbon 62, 779–820. https://doi.org/10.1017/RDC.2020.68.

Hernaiz Huerta, P.P., García de Domingo, A., González-Lastras, J., Zazo Cerdeña, C., Goy Goy, J.L., 1991. *Cartografía geológica y memoria de la hoja 13–47 (Tahivilla)*. Mapa Geológico de España, Escala 1:50.000. Plan MAGNA, 2ª Serie, Madrid, Spain, p. 45. IGME.

Hernández-Pacheco, E., Cabré, J., 1913. La Depresión del Barbate y sus estaciones prehistóricas. Bol. R. Soc. Esp. Hist. Nat. 13, 349–359. https://bibdigital.rjb.csic.es/records/item/10562-boletin-de-la-real-sociedad-espanola-de-historia-natural-tomo-13?offset=.

Hidrográfico de la Marina, Instituto, 2019. Anuario de Mareas 2020. Regional 4. De la desembocadura del río Guadiana al Estrecho de Gibraltar. Ministerio de Defensa de España, Madrid, p. 46. https://publicaciones.defensa.gob.es/media/downloadable/files/links/a/n/anuario_mareas_regional_4_2020.pdf.

Hindson, R., Andrade, C., Parish, R., 1998. A microfaunal and sedimentary record of environmental change within the late Holocene sediments of Boca do Rio (Algarve, Portugal). Geol. Mijnbouw 77, 311–321. https://doi.org/10.1023/A:1003651308741.

Imbrie, J., McIntyre, A., Mix, A., 1989. Oceanic response to orbital forcing in the late quaternary: observational and experimental strategies. In: Berger, A., Schneider, S., Duplessy, J.C. (Eds.), Climate and Geo-Sciences, NATO ASI Series, vol. 285. Springer, Dordrecht, pp. 121–164. https://doi.org/10.1007/978-94-009-2446-8_7.

Lambeck, K., Rouby, H., Purcell, A., Sun, Y., Sambridge, M., 2014. sea level and global ice volumes from the last glacial maximum to the Holocene. Proceedings of the National Academy of Sciences USA 111, 15296–15303. https://doi.org/10.1073/pnas.1411762111.

Lario, J., Zazo, C., Goy, J.L., Dabrio, C.J., Borja, F., Silva, P.G., Sierro, F., González, A., Soler, V., Yil, E., 2002. Changes in sedimentation trends in SW Iberia Holocene estuaries (Spain). Quat. Int. 93–94, 171–176. https://doi.org/10.1016/S1040-6182(02)00015-0.

Latorre, A.V.P., Mera, A. G. de, Dell, U., Cabezudo, B., 1996. Fitogeografía y vegetación del Sector Aljíbico (Cádiz-Málaga, España). Acta Bot. Malacitana 21, 241–267. https://doi.org/10.24310/abm.v21i0.8678.

Leblanc, D., 1990. Tectonic adaptation of the External Zones around the curved core of an orogen: the Gibraltar Arc. J. Struct. Geol. 12, 1013–1018. https://doi.org/10.1016/0191-8141(90)90097-I.

Lisiecki, L.E., Raymo, M.E., 2005. A Pliocene-Pleistocene stack of 57 globally distributed benthic $\delta^{18}O$ records. Paleoceanography 20, PA1003. https://doi.org/10.1029/2004PA001071.

Lobo, F.J., Días, J.M.A., González, R., Hernández-Molina, F.J., Morales, J.A., Díaz del Río, V., 2003. High-resolution seismic stratigraphy of a narrow, bedrock-controlled estuary: the Guadiana estuarine system, SW iberia. J. Sediment. Res. 73, 973–986. https://doi.org/10.1306/032303730973.

López-Sáez, J.A., Van Geel, B., Martín-Sánchez, M., 2000. Aplicación de los microfósiles no polínicos en Palinología Arqueológica. In: Oliveira, Jorge, (coord, V. (Eds.), Contributos das Ciências e das Technologias para a Arqueologia da Península Ibérica, Actas 3° Congresso de Arqueologia Peninsular, vol. 9, pp. 11–20.

Luque, L., Zazo, C., Recio, J.M., Dueñas, M.A., Goy, J.L., Lario, J., González-Hernández, F., Dabrio, C.J., González-Delgado, A., 1999. Evolución sedimentaria de la laguna de La Janda (Cádiz) durante el Holoceno. Cuaternario Geomorfol. 13, 43–50.

Luque, L., Silva, P.G., Zazo, C., Recio, J.M., Carrasco, P., Goy, J.L., Dueñas, M.I., Lario, J., Dabrio, C.J., González-Hernández, F.M., Poza, L., 2001. Datos geofísicos y evolución sedimentaria de la Depresión de La Janda (Cádiz). Geogaceta 29, 69–72.

Lyle, M., 1983. The brown-green color transition in marine sediments: a marker of the Fe (III)-Fe(II) redox boundary. Limnol. Oceanogr. 28, 1026–1033. https://doi.org/10.4319/lo.1983.28.5.1026.

Martins, J.M.M., Soares, A.M.M., 2013. Marine radiocarbon reservoir effect in southern atlantic iberian coast. Radiocarbon 55, 1123–1134. https://doi.org/10.1017/S0033822200048037.

Mendes, I., Lobo, F.J., Hanebuth, T.J.J., López-Quirós, A., Schönfeld, J., Lebreiro, S., Reguera, M.I., Antón, L., Ferreira, O., 2020. Temporal variability of flooding events of Guadiana River (Iberian Peninsula) during the middle to late Holocene: imprints in the shallow-marine sediment record. Palaeogeogr. Palaeoclimatol. Palaeoecol. 556, 109900 https://doi.org/10.1016/j.palaeo.2020.109900.

Menier, D., Tessier, B., Proust, J.-N., Baltzer, A., Sorrel, P., Traini, C., 2010. The Holocene transgression as recorded by incised-valley infilling in a rocky coast context with low sediment supply (southern Brittany, western France). Bull. Soc. Geol. Fr. 181, 115–128. https://doi.org/10.2113/gssgfbull.181.2.115.

Moore, P.D., Webb, J.A., Collinson, M.E., 1991. Pollen Analysis. Blackwell Science, p. 216.

Morales, J.A., 1997. Evolution and facies architecture of the mesotidal Guadiana River delta (S.W. Spain-Portugal). Mar. Geol. 138, 127–148. https://doi.org/10.1016/S0025-3227(97)00009-1.

Morales, J.A., Delgado, I., Gutierrez-Mas, J.M., 2006. Sedimentary characterization of bed types along the Guadiana estuary (SW Europe) before the construction of the Alqueva dam. Estuar. Coast Shelf Sci. 70, 117–131. https://doi.org/10.1016/j.ecss.2006.05.049.

Nagao, S., Nakashima, S., 1992. The factors controlling vertical color variations of North Atlantic Madeira Abyssal Plain sediments. Mar. Geol. 109, 83–94. https://doi.org/10.1016/0025-3227(92)90222-4.

Nicholls, R.J., Hanson, S.E., Lowe, J.A., Slangen, A.B.A., Wahl, T., Hinkel, J., Long, A.J., 2021. Integrating new sea-level scenarios into coastal risk and adaptation assessments: an ongoing process. WIREs Climate Change 12, e706. https://doi.org/10.1002/wcc.706.

Past Interglacials Working Group of PAGES, 2016. Interglacials of the last 800,000 years. Rev. Geophys. 54, 162–219. https://doi.org/10.1002/2015RG000482.

Poirier, C., Tessier, B., Chaumillon, E., 2017. Climate control on late Holocene high-energy sedimentation along coasts of the northeastern Atlantic Ocean. Palaeogeogr. Palaeoclimatol. Palaeoecol. 485, 784–797. https://doi.org/10.1016/j.palaeo.2017.07.037.

Posamentier, H.W., Vail, P.R., 1988. Eustatic control on clastic deposition: II sequence and system tract models. In: Wilgus, C.K., Hastings, B.S., Kendall, C.G.StC., Posamentier, H.W., Ross, C.A., Van Wagoner, J.C. (Eds.), Sea Level Changes – an Integrated Approach, vol. 42. SEPM Special Publication, pp. 125–154. https://doi.org/10.2110/pec.88.01.0125.

Reicherter, K.R., Peters, G., 2005. Neotectonic evolution of the central betic Cordilleras (southern Spain). Tectonophysics 405, 191–212. https://doi.org/10.1016/j.tecto.2005.05.022.

Reille, M., 1992. Pollen et spores d'europe et d'afrique du nord. Éditions du Laboratoire de Botanique historique et Palynologie, Marseille, p. 520.

Reille, M., 1995. Pollen et Spores d'Europe et d'Afrique du Nord. Éditions du Laboratoire de Botanique historique et Palynologie, Marseille, p. 327. Supplement 1.

Reimer, R.W., Reimer, P.J., 2017. An online application for ΔR calculation. Radiocarbon 59, 1623–1627. http://calib.org/JS/JSdeltar20/. (Accessed 26 January 2021).

Reimer, P.J., Austin, W.E.N., Bard, E., Bayliss, A., Blackwell, P.G., Bronk Ramsey, C., Butzin, M., Cheng, H., Edwards, R.L., Friedrich, M., Grootes, P.M., Guilderson, T.P., Hajdas, I., Heaton, T.J., Hogg, A.G., Hughen, K.A., Kromer, B., Manning, S.W., Muscheler, R., Palmer, J.G., Pearson, C., van der Plicht, J., Reimer, R.W., Richards, D.A., Scott, E.M., Southon, J.R., Turney, C.S.M., Wacker, L., Adolphi, F., Büntgen, U., Capano, M., Fahrni, S.M., Fogtmann-Schulz, A., Friedrich, R., Köhler, P., Kudsk, S., Miyake, F., Olsen, J., Reinig, F., Sakamoto, M., Sookdeo, A., Talamo, S., 2020. The IntCal20 northern hemisphere radiocarbon age calibration curve (0–55 cal kBP). Radiocarbon 62, 725–757. https://doi.org/10.1017/RDC.2020.41.

Rivas-Martínez, S., Asensi, A., Diez-Garretas, B., Molero, J., Valle, F., 1997. Biogeographical synthesis of andalusia (southern Spain). J. Biogeogr. 24, 915–928. https://doi.org/10.1046/j.1365-2699.1997.00149.x.

Rodríguez-Vidal, J., Cáceres, L.M., Finlayson, J.C., Garcia, F.J., Martínez-Aguirre, A., 2004. Neotectonics and shoreline history of the Rock of Gibraltar, south Iberia. Quat. Sci. Rev. 23, 2017–2029. https://doi.org/10.1016/j.quascirev.2004.02.008.

Roldán, F.J., Rodríguez-Fernández, J., Villalobos, M., Lastra, J., Díaz-Pinto, G., Pérez Rodríguez, A.B., 2021. Mapa Geológico Digital continuo E. 1:50.000, Zonas: subbético, Cuenca del Guadalquivir y Campo de Gibraltar. In: GEODE. Mapa Geológico Digital continuo de España [online]. [02/november/2021]. http://info.igme.es/cartografiadigital/geologica/geodezona.aspx?Id=Z2600.

Ruiz, F., Rodríguez-Ramírez, A., Cáceres, L.M., Rodríguez-Vidal, J., Carretero, M.I., Clemente, L., Muñoz, J.M., Yáñez, C., 2004. Late Holocene evolution of the southwestern doñana national park (guadalquivir estuary, SW Spain): a multivariate approach. Palaeogeogr. Palaeoclimatol. Palaeoecol. 204, 47–64. https://doi.org/10.1016/S0031-0182(03)00721-1.

Sanz de Galdeano, C., 1990. Geologic evolution of the betic Cordilleras in the western mediterranean, Miocene to the present. Tectonophysics 172, 107–119. https://doi.org/10.1016/0040-1951(90)90062-D.

Schneider, H., Höfer, D., Trog, C., Busch, S., Schneider, M., Baade, J., Daut, G., Mäusbacher, R., 2010. Holocene estuary development in the Algarve Region (Southern Portugal) - a reconstruction of sedimentological and ecological evolution. Quat. Int. 221, 141–158. https://doi.org/10.1016/j.quaint.2009.10.004.

Soares, A.M.M., Dias, J.M.A., 2006. Coastal upwelling and radiocarbon evidence for temporal fluctuations in ocean reservoir effect off Portugal during the Holocene. Radiocarbon 48, 45–60. https://doi.org/10.1017/S0033822200035384.

Soares, A.M.M., Martins, J.M.M., 2010. Radiocarbon dating of marine samples from Gulf of Cadiz: the reservoir effect. Quat. Int. 221, 9–12. https://doi.org/10.1016/j.quaint.2009.10.012.

Soulet, G., 2015. Methods and codes for reservoir-atmosphere 14C age offset calculations. Quat. Geochronol. 29, 97–103. https://doi.org/10.1016/j.quageo.2015.05.023.

Spratt, R.M., Lisiecki, L.E., 2016. A Late Pleistocene sea level stack. Clim. Past 12, 1079–1092. https://doi.org/10.5194/cp-12-1079-2016.

Stockmarr, J., 1971. Tablets with spores used in absolute pollen analysis. Pollen Spores 13, 615–621.

Strauss, B.H., Kulp, S.A., Rasmussen, D.J., Levermann, A., 2021. Unprecedented threats to cities from multi-century sea level rise. Environ. Res. Lett. 16, 114015 https://doi.org/10.1088/1748-9326/ac2e6b.

Stuiver, M., Reimer, P.J., Reimer, R.W., 2021. CALIB 8.2 [WWW program] at. http://calib.org. (Accessed 14 September 2021).

Tjallingii, R., Röhl, U., Kölling, M., Bickert, T., 2007. Influence of the water content on X-ray fluorescence core-scanning measurements in soft marine sediments. G-cubed 8, Q02004. https://doi.org/10.1029/2006GC001393.

Val-Peón, C., López-Sáez, J.A., Santisteban, J.I., Mediavilla, R., Becerra, S., Domínguez, S., Fernández-Sánchez, D.S., Ramos Muñoz, J., Vijande Vila, E., Cantillo Duarte, J.J., Reicherter, K. (this volume). Natural and Anthropogenic Processes in the Depression of La Janda (SW Iberia) from the Late Pleistocene to the Mid-late Holocene.

Van Geel, B., 1978. A palaeoecological study of Holocene peat bog sections in Germany and The Netherlands, based on the analysis of pollen, spores and macro- and microscopic remains of fungi, algae, cormophytes and animals. Rev. Palaeobot. Palynol. 25, 1–120. https://doi.org/10.1016/0034-6667(78)90040-4.

Van Geel, B., 2001. Non-pollen palynomorphs. In: Smol, J.P., Birks, H.J.B., Last, W.M., Bradley, R.S., Alverson, K. (Eds.), Tracking Environmental Change Using Lake

Sediments: Terrestrial, Algal, and Siliceous Indicators. Springer Netherlands, pp. 99–119. https://doi.org/10.1007/0-306-47668-1_6.

Van Geel, B., Klink, A.G., Pals, J.P., Wiegers, J., 1986. An Upper Eemian lake deposit from Twente, eastern Netherlands. Rev. Palaeobot. Palynol. 47, 31–61. https://doi.org/10.1016/0034-6667(86)90005-9.

Van Geel, B., Bohncke, S.J.P., Dee, H., 1980. A palaeoecological study of an upper late glacial and holocene sequence from "de borchert", The Netherlands. Rev. Palaeobot. Palynol. 31, 367–448. https://doi.org/10.1016/0034-6667(80)90035-4.

Van Geel, B., Buurman, J., Brinkkemper, O., Schelvis, J., Aptroot, A., van Reenen, G., Hakbijl, T., 2003. Environmental reconstruction of a Roman Period settlement site in Uitgeest (The Netherlands), with special reference to coprophilous fungi. J. Archaeol. Sci. 30, 873–883. https://doi.org/10.1016/S0305-4403(02)00265-0.

Van Geel, B., Coope, G.R., Van Der Hammen, T., 1989. Palaeoecology and stratigraphy of the late glacial type section at Usselo (The Netherlands). Rev. Palaeobot. Palynol. 60, 25–129. https://doi.org/10.1016/0034-6667(89)90072-9.

Van Wagoner, J.C., Posamentier, H.W., Mitchum, R.M., Vail, P.R., Sarg, J.F., Loutit, T.S., Hardenbol, J., 1988. An overview of the fundamentals of sequence stratigraphy and key definitions. In: Wilgus, C.K., Hastings, B.S., Kendall, C.G.StC., Posamentier, H. W., Ross, C.A., Van Wagoner, J.C. (Eds.), Sea Level Changes – an Integrated Approach, vol. 42. SEPM Special Publication, pp. 39–45. https://doi.org/10.2110/pec.88.01.0039.

Vergés, J., Fernández, M., 2012. Tethys-Atlantic interaction along the Iberia-Africa plate boundary: the Betic-Rif orogenic system. Tectonophysics 579, 144–172. https://doi.org/10.1016/j.tecto.2012.08.032.

Zaitlin, B.A., Dalrymple, R.W., Boyd, R., 1994. The stratigraphic organization of incised-valley systems associated with relative sea-level change. In: Dalrymple, R.W., Boyd, R., Zaitlin, B.A. (Eds.), Incised-valley Systems: Origin and Sedimentary Sequences, vol. 51. SEPM Special Publication, pp. 45–60. https://doi.org/10.2110/pec.94.12.0045.

Zazo, C., Silva, P.G., Goy, J.L., Hillaire-Marcel, C., Ghaleb, B., Lario, J., Bardají, T., González, A., 1999. Coastal uplift in continental collision plate boundaries: data from the Last Interglacial marine terraces of the Gibraltar Strait area (south Spain). Tectonophysics 301, 95–109. https://doi.org/10.1016/S0040-1951(98)00217-0.

Ziegler, M., Jilbert, T., de Lange, G.J., Lourens, L.J., Reichart, G.J., 2008. Bromine counts from XRF scanning as an estimate of the marine organic carbon content of sediment cores. G-cubed 9, Q05009. https://doi.org/10.1029/2007GC001932.